International Journal of Pharmaceutics 686 (2025) 126320

Contents lists available at ScienceDirect

International Journal of Pharmaceutics

journal homepage: www.elsevier.com/locate/ijpharm

Antimicrobial casein/poly(vinyl alcohol) electrospun nanofibers-based dressings

D. Nobre [a,1], E. Ekoh [a,1], D.C. Silva [a], A.C. Branco [a,b], V. Pais [c], A. Almeida [d], H. Barroso [e], M. Salema-Oom [e], R. Fangueiro [c,f], R. Colaço [b], R. Galante [g,*], A.P. Serro [a,e,**]

[a] Centro de Química Estrutural (CQE), Chemical Engineering Department and Institute of Molecular Sciences, Instituto Superior Técnico, University of Lisbon, Av. Rovisco Pais 1, 1049-001 Lisbon, Portugal
[b] Instituto de Engenharia Mecânica (IDMEC), Department of Mechanical Engineering, Instituto Superior Técnico, University of Lisbon, Av. Rovisco Pais 1, 1049-001 Lisbon, Portugal
[c] Associação Fibernamics - Instituto de Inovação em Materiais Fibrosos e Compósitos, Universidade do Minho, Campus Azurém, 4800-058 Guimarães, Portugal
[d] Center of Physics and Engineering of Advanced Materials (CeFEMA) and Chemical Engineering Department, Instituto Superior Técnico, University of Lisbon, Av. Rovisco Pais 1, 1049-001 Lisbon, Portugal
[e] Egas Moniz Centre for Interdisciplinary Research (CiiEM), Egas Moniz School of Health & Science, Campus Universitário, Quinta da Granja, 2829-511 Monte de Caparica, Almada, Portugal
[f] Department of Mechanical Engineering, University of Minho, Campus de Azurém, Av. da Universidade, 4800-058 Guimarães, Portugal
[g] Centro de Inovação em Materiais e Produtos Avançados, (CIMPA), Rua da Tecnologia K - Epsilon 2, 9560-421 Rosário, Lagoa (São Miguel - Azores), Portugal

ARTICLE INFO

Keywords:
Casein
Nanofibers
Electrospinning
Wound dressings
Antimicrobial properties

ABSTRACT

Diabetes affects millions globally, with a rising prevalence. Chronic wounds are one of its major complications, due to the healing difficulty, highlighting the need for innovative solutions to improve the treatments efficacy. Electrospun nanofiber dressings show promising due to their ECM-like structure, oxygen permeability, and potential for bioactive functionalization. In this study, casein/poly(vinyl alcohol) (CAS/PVA) nanofibers were electrospun with antimicrobial compounds: Octiset®, polyhexanide, and ZnO particles. After crosslinking with glutaraldehyde (GA), the nanofibers mats were characterized regarding their morphology, swelling capacity, enzymatic degradation, drug release behavior, cytotoxicity, hemocompatibility, irritability potential and antimicrobial potential. They demonstrated notable swelling capacity, and therefore potential to absorb exudate and maintain a moist healing environment in the wound. Those containing polyhexanide and Octiset® (CAS/PVA_Poli and CAS/PVA_Octi) showed a significant drug release for over 4–8 h, that prolonged at a slower rate for 24 h, being mainly diffusion-controlled. The crosslinker reduced the amount of drug released and the degradation of the nanofibers but increased their water absorption capacity. CAS/PVA_Poli and CAS/PVA_Octi exhibited the most interesting set of results, as besides being non-cytotoxicity, hemocompatible and non-irritant, presented excellent antimicrobial efficacy and superior performance when compared with the crosslinked samples. They were effective against *Staphylococcus aureus*, *Escherichia coli*, and *Candida albicans,* and in particular against Methicillin Resistant *Staphylococcus aureus* and *Streptococcus pyogenes* which are a dangerous threat in diabetic wounds. Overall, their morphological similarity with the extracellular matrix and excellent biological properties, turns them good candidates to be used in dressings for the treatment of diabetic wounds.

1. Introduction

The prevalence of diabetes mellitus (DM), which is already experiencing an upward trend, is anticipated to continue growing over the coming decades. In fact, in 2024, the global prevalence of DM among adults aged 20 to 79 was estimated at 11.1 %, affecting approximately 589 million individuals. Projections indicate that by 2050, the number of adults with diabetes could rise to 853 million, i.e., 1 in 8 adults

* Corresponding author.
** Corresponding author at: Centro de Química Estrutural (CQE), Chemical Engineering Department and Institute of Molecular Sciences, Instituto Superior Técnico, University of Lisbon, Av. Rovisco Pais 1, 1049-001 Lisbon, Portugal.
E-mail addresses: raquelgalante@cimpa.pt, rakelgalante@gmail.com (R. Galante), anapaula.serro@tecnico.ulisboa.pt (A.P. Serro).
[1] First co-authors.

https://doi.org/10.1016/j.ijpharm.2025.126320
Received 19 August 2025; Received in revised form 24 October 2025; Accepted 26 October 2025
Available online 30 October 2025

worldwide (Diabetes around the world-2024). Furthermore, DM is responsible for a death every six seconds and has contributed to a 338 % surge in healthcare expenditures over the past 17 years, totalling USD 1.015 trillion in global health costs (Diabetes around the world-2024). In short, DM poses substantial global health and social concerns (Singer et al., 2022), giving rise to significant challenges for patients, families, and societies alike (Bommer et al., 2018).

Diabetic foot ulcers (DFUs) represent one of the most severe and incapacitating consequences of diabetes, impacting 15 to 25 % of DM patients throughout their lifetimes (Akkus and Sert, 2022). In 85 % of cases, these ulcers become infected with multiple microorganisms, rendering them unresponsive to treatment and requiring prolonged hospitalization and even amputations (Mahgoub et al., 2022; Aydın et al., 2024). Present approaches to manage DFUs emphasize interdisciplinary approaches, addressing vital aspects of diabetic wound care, such as the regulation of blood sugar levels, ensuring adequate blood flow, removing necrotic tissue, alleviating pressure, and managing infections (Zhang et al., 2023; Da Silva et al., 2023; Kurze et al., 2022). In order to enhance the management of this condition and consequently attain higher rates of treatment success, the exploration of more potent therapeutic alternatives becomes imperative.

In recent years, great progress has been made in the field of skin repair and tissue engineering (Zhang et al., 2023; Tavakoli and Klar, 2020). In particular, there has been high interest/demand for alternative and sustainable raw materials. Structures such as films, foams, hydrogels, scaffolds, hydrocolloids, and nanofibers have been produced and investigated for the treatment of acute and chronic wounds (Maaz Arif et al., 2021). In this sense, technologies such as electrospinning (Tonda-Turo et al., 2018; Liu et al., 2021; Rediguieri et al., 2016; Fahimirad et al., 2024; Aliee et al., 2025) have been reported as great tools to achieve a structural organization similar to the tissues, that may benefit the healing process. Furthermore, the biomimetic functionalization approach could enable the development of a system that mimics both the architectural and biochemistry environment of the live tissues. This can be achieved by incorporating bioactive agents, such as growth factors (Mariia et al., 2021; Sahoo et al., 2010), antioxidants (Fitzmaurice et al., 2011), antibacterial and anti-inflammatories (Homaeigohar and Boccaccini, 2020; Shahriar et al., 2019), among others (Miguel et al., 2019). The high surface area of nanofibers enhances their biodegradability, allowing for sustained delivery of these agents.

Milk proteins, such as casein (CAS) and whey, have deserved an increased attention due to the presence of active peptides encrypted within their structure (Purup et al., 2019). These peptides are known to have antihypertensive, opioid, immunomodulatory, antithrombotic and antimicrobial effects (Purup et al., 2019; Pouliot and Gauthier, 2006). Caseins in particular, are biocompatible, biodegradable, as well as highly stable and non-toxic (Rehan et al., 2019). They stimulate the proliferation of human lymphocytes, antibody synthesis and phagocytosis. Additionally, they promote the proliferation of natural killer cells and T cells, enhancing the body's defence mechanisms against a wide range of bacteria (Ahmed et al., 2023). These phosphoproteins present a great versatility and may be used in a variety of forms: films, hydrogels, micelles, micro and nanoparticles as well as micro and nanofibers (Rehan et al., 2019; Selvaraj et al., 2018).

CAS alone is generally not easily electrospinnable, due to its low molecular weight which leads to low viscosity solutions and to the formation of beads instead of continuous fibre structures. To address this issue, casein can be mixed with other polymers, like polyvinyl alcohol (PVA), a biodegradable, water soluble, nontoxic and biocompatible polymer, to increase the solution's viscosity, its electrospinnability and uniformity of the obtained nanofibers (Durmaz and Aytac, 2019). It improves the mechanical strength and flexibility of the nanofibers, making them more durable and suitable for wound care. Besides it contributes to control the material's degradation, ensuring that the dressing keeps its function. Additionally, PVA helps maintaining a moist wound environment, essential to promote a faster healing.

This work aimed to produce a multifunctional wound dressing based on CAS and PVA for the treatment of diabetic wounds. A double strategy was followed:

(1) The extracellular matrix (ECM) structure was mimicked by producing CAS/PVA electrospun nanofibers that can support cell adhesion, proliferation, and differentiation. The combination of the two polymers shall confer ideal properties to the wound dressing. On the one hand, both are biocompatible, which reduces the risk of adverse reactions. On the other hand, the blend provides optimal mechanical strength and flexibility, essential for wound protection and comfort.

(2) To control infection at the wound site, several antimicrobial agents were incorporated onto the matrix: Octiset® (a combination of octenidine dihydrochloride with 2-phenoxyethanol), polyhexanide and zinc oxide (ZnO). The chemical structure of these bioactive agents is shown in Fig. 1. The use of all these antimicrobial compounds in wound care is advantageous due to its long-lasting effect and minimal resistance development, making them a reliable choice for preventing and managing infections at the wound site.

Octenidine dihydrochloride is an antimicrobial substance characterized by its two non-interacting cationic-active centres, separated by a long aliphatic hydrocarbon chain. Due to its cationic nature, it interacts strongly with the negatively charged components of microbial cell walls and membranes and can react with them, disrupting the enzymatic systems and leading to cytoplasmic membrane leakage, which may compromise cell function. Octenidine presents a broad antimicrobial activity against Gram-positive and Gram-negative bacteria (Chiaula et al., 2023). Its efficacy can be enhanced when used in combination with 2-phenoxyethanol, a preservative that helps stabilizing aqueous formulations, enhancing octenidine solubility, and also presents antimicrobial activity (Szostak et al., 2018).

Polyhexanide, also known as polyhexamethylene biguanide (PHMB), is another cationic polymer that can disrupt microbial membranes by attaching to negatively charged membrane lipids, leading to increased membrane permeability. PHMB is effective against a broad spectrum of pathogens, including Gram-positive and Gram-negative bacteria, as well as fungi, molds and yeasts (Guiomar and Urbano, 2022).

Zinc oxide (ZnO) presents strong antibacterial properties and supports tissue regeneration, making it a valuable component in managing and promoting wound healing. Besides, its anti-inflammatory and astringent effects are well established (Raha and Ahmaruzzaman, 2022).

In order to increase the stability and physical properties of the nanofibers, crosslinking with glutaraldehyde (GA) vapor was performed, giving rise to the reaction shown in Fig. 2. GA is a bifunctional aldehyde that can readily react with amine groups of casein (Głąb and Boratyński, 2017) and with the hydroxyl groups of PVA as shown in Fig. 2 (Musa and Hameed, 2021). Its use in vapor form allows for uniform crosslinking of nanofibers matrix and can help maintaining their structural integrity, which could be compromised by crosslinking with liquids. Besides, it can minimize the amount of residual GA within the matrix, decreasing the risk of cytotoxicity.

The release of the antimicrobial agents (except ZnO) from the produced nanofiber matrix was evaluated in sink conditions. The different systems were characterized in terms of morphology, swelling, and degradation. Furthermore, irritability, cytotoxicity, hemocompatibility and antimicrobial tests against different microorganisms were carried out to conclude about the suitability of the materials to be used in wound dressings.

2. Materials and Methods

2.1. Materials

Casein from bovine milk, zinc oxide dispersion (nanoparticles < 100 nm particle size) and glutaraldehyde (GA) solution Grade II (25 % in H_2O) were obtained from Merck. Triethanolamine was purchased from PanReac AppliChem. Poly(vinyl alcohol) (PVA) Mw 145 000 LA (Poval

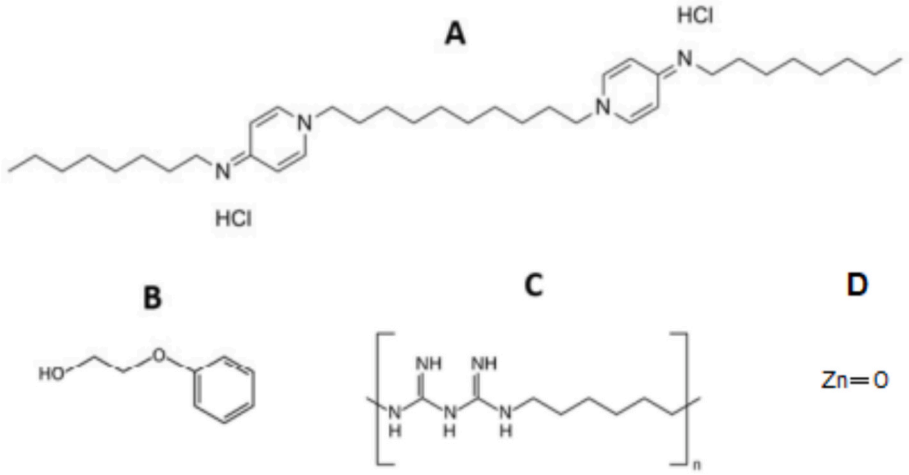

Fig. 1. Chemical structure of (A) octenidine dihydrochloride, (B) 2-phenoxyethanol, (C) polyhexanide and (D) zinc oxide.

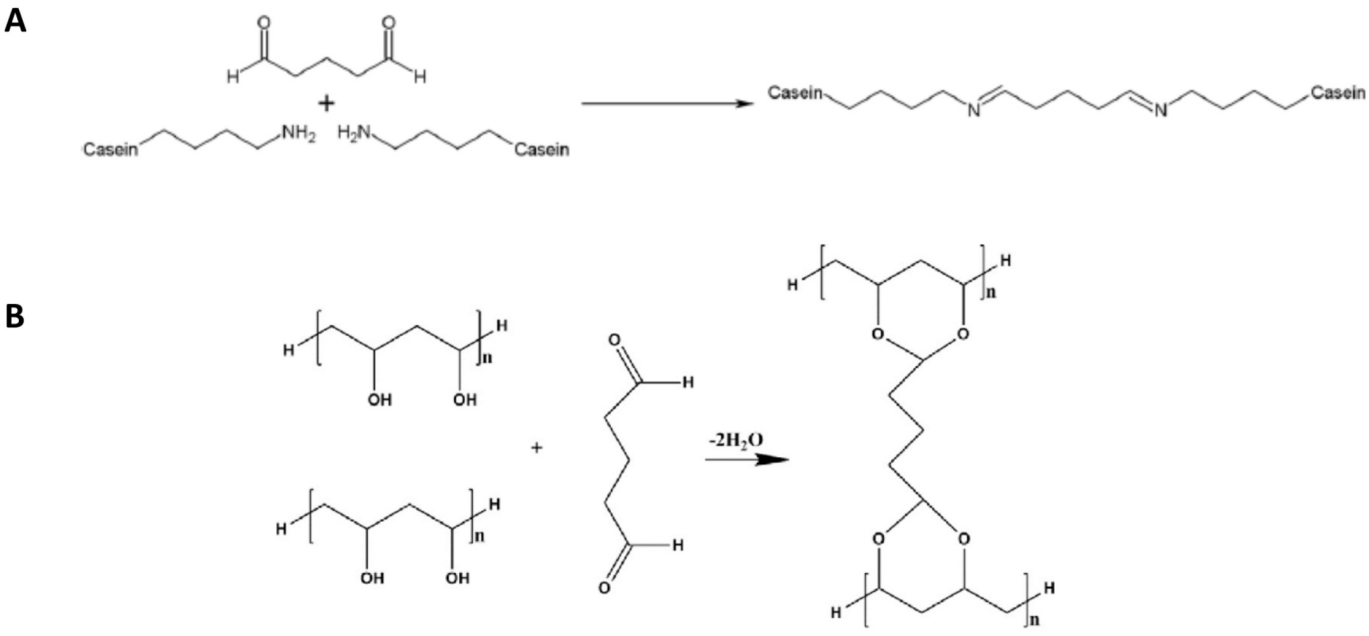

Fig. 2. Crosslinking of (A) casein and (B) PVA with glutaraldehyde (GA).

28–99 LA) was obtained from Kuraray. Octiset® commercial solution, containing two active substances, 2-phenoxyethanol in a concentration of 20 mg/mL and octenidine dihydrochloride in a concentration of 1 mg/mL, was obtained from Schulke. Polyhexanide was obtained from Carbosynth. Phosphate buffered saline (PBS) tablets were supplied by Sigma and dissolved in distilled and deionized (DD) water. Protease from *Streptomyces griseus* (Type XIV $\geq$ 3.5 units/mg) used in the degradation assay was purchased from Sigma. The culture medium used in the antimicrobial activity tests was the Mueller-Hinton Broth (MHB, CM0405, OXOID). NIH/3T3 fibroblasts (93061524), Dulbecco's Modified Eagle's Medium (DMEM), bovine calf serum, penicillin–streptomycin solution, trypsin, EDTA (ethylenediaminetetraacetic acid) solution, dimethyl sulfoxide (DMSO), MTT solution (3-(4,5-dimethylthiazol-2-yl)-2,5-diphenyltetrazoliumbromid) and the hydrochloric acid and isopropanol used in cytotoxic test were obtained from Sigma. Lastly, IGEPAL (octylphenoxy poly(ethyleneoxy) ethanol) was purchased from Merck.

2.2. Methods

2.2.1. Electrospinning solution preparation

Four different formulations were processed. For the first, CAS/PVA, a PVA solution (5 % w/v) was prepared in DD water at 90 °C under magnetic stirring for 2 h and then cooled to room temperature. Then, 16 % (w/v) casein was dissolved in water containing 4 % v/v of triethanolamine, at room temperature and with magnetic stirring at 300 rpm for 8 h. The casein solution was left overnight for degassing. Next, both solutions were mixed to obtain CAS/PVA composition of 60/40 mass ratios. CAS/PVA_Octi was prepared following the same procedure, however, instead of water, an Octiset® commercial solution was used to dissolve PVA. For CAS/PVA_Poli, the 5 % (w/v) PVA solution was prepared in water containing 0.1 % (w/v) polyhexanide. Finally, CAS/PVA_ZnO was prepared by suspending 1 % (w/v) ZnO nanoparticles in the casein/PVA solution prepared as in CAS/PVA.

2.2.2. Electrospinning solution viscosity

The electrospinning solutions' viscosities were measured with a

Rheometer MCR 92 (from Anton Paar) equipped with a CP50-1 cone plate at a shear rate of 1–100 s^{-1} with the controlled temperature of 25 °C. The software Rheocompass was used to obtain the viscosity curves and analyse the data. The assays were performed in triplicated for each system.

2.2.3. Nanofibers electrospinning

The nanofibers were prepared based on a protocol adapted from (Biranje et al., 2019; Yeniay et al., 2019). Briefly, casein/PVA solutions were electrospun using a syringe pump NE-300 New Era Pump systems. The power source was from GenVolt high voltage power supply 73,030 (output voltage: 0–30 kV) and the collector used was a stationary flat target collector covered with aluminium foil. The voltage was fixed at 25 kV, the distance to collector was 10 cm, and the flow rate was set to 0.5 mL/h. A flat-tip standard hypodermic needle 18G was used and the deposition time was 2 h. Nanofiber samples were used in the subsequent assays having as support the aluminium foil.

2.2.4. Nanofibers crosslinking

The produced nanofibers were crosslinked with GA vapor to decrease their solubility. The procedure consisted in keeping the samples for 5 h at room temperature inside a recipient with a saturated environment in GA. This was achieved by placing in the bottom of the recipient a GA solution (25 % in DD water) that was not in contact with the samples. Then, the crosslinked nanofibers were put in a vacuum oven for 3 days to remove GA traces (Selvaraj et al., 2018). The crosslinked nanofibers will be named using the suffix GA.

The overall procedure to produce the nanofibers since the solutions formulation till the crosslinking procedure is resumed in Fig. 3.

2.2.5. Sterilization

Samples were sterilized by gamma irradiation using radioactive Cobalt-60. They were sealed in special bags (polyamide and polyethylene, 90 μm thickness) and submitted to the standard dose of 25 kGy with a dose rate of 5 $kGy.h^{-1}$.

2.2.6. Morphology

The nanofibers surface morphology was studied using a scanning electron microscope (SEM) JEOL 7001F operating at 15 kV. All samples were coated with gold/palladium by sputtering before imaging. The average diameter of the nanofibers was measured using the software Digimizer by taking at least 100 random measurements per image ($n \geq 100$).

2.2.7. Swelling

Discs with 8 mm of diameter of the supported nanofibers were cut and weighted. Samples were then immersed in 10 mL of PBS solution at room temperature. At specific time intervals, they were withdrawn from the PBS, carefully blotted to remove the excess water, and weighted again. The swelling ratio was calculated, according to equation (1):

$$Swelling(\%) = \frac{W_s - W_d}{W_d} \times 100 \quad (1)$$

where (W_s) is the weight of swollen nanofibers and (W_d) is the weight of dried ones, obtained discounting to the measured values, the weight of bare aluminium foil discs with the same dimensions. Experiments were

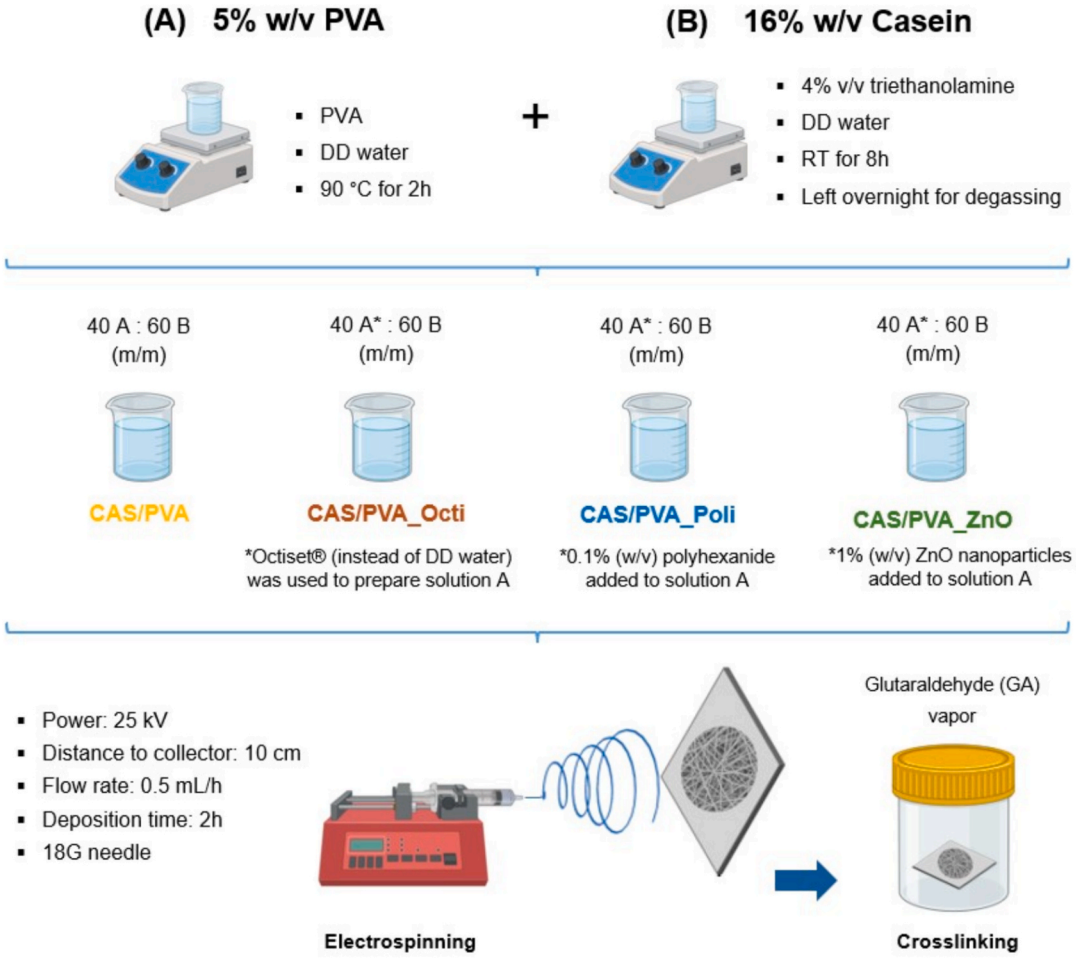

Fig. 3. Scheme of the experimental procedure to produce the nanofibers.

carried out at least in triplicate.

2.2.8. Drug release

Samples with 15 mm of diameter were cut and mounted into Franz Cells with the nanofibers facing the receptor chamber full of PBS. The drug release profiles were obtained as follows: at specific time intervals, 200 μL of the receptor solution were withdrawn from the cell and replaced with an equal volume of fresh PBS. The drug content in the collected aliquots was quantified by UV–Vis Spectrometry, at 220 nm for phenoxyethanol and polyhexanide and 270 nm for octenidine dihydrochloride (Spectrophotometer Multiskan® GO UV/Vis from Thermo Scientific). ($N \geq 3$).

2.2.9. Degradation behavior

The degradation of the nanofibers was performed in an enzymatic solution. Samples with 8 mm of diameter were weighed, immersed in 10 mL of PBS containing 0.2 mg/ml of protease enzyme XIV solution kept at 37 °C for 24 h. Then, they were blotted to remove the excess of solution, freeze-dried for 24 h and weighed again. The weight loss was calculated, according to the equation (2) (Çay et al., 2014):

$$Weightloss(\%) = \frac{W_0 - W_1}{W_0} \times 100 \quad (2)$$

where W_0 is the initial weight of the samples and W_1 is the weight of dried samples, both corrected by subtraction of the weight of an aluminium disc with the same dimensions. Measurements were done at least in triplicate ($n \geq 3$).

2.2.10. Chemical structure

The chemical structure of the fibres was analysed using Fourier Transform Infrared Spectroscopy (FTIR) with an Attenuated Total Reflectance (ATR) accessory. FTIR spectra were recorded in the 4000–850 cm^{-1} wavenumber range at a resolution of 1 cm^{-1} using a Spectrum Two FT-IR spectrometer (PerkinElmer®, USA). Spectra of the raw materials were also obtained for comparison. Data were normalized using Prism 9.5.1 (GraphPad Software, USA). Each spectrum represents the average of three replicates.

2.2.11. Crystallinity

The X-ray diffraction analysis of nanofibers mats deposited on aluminium foil was performed using a Bruker D8 Advance diffractometer, operated at 40 kV, 30 mA. The experiments were carried out with Cu-Kα radiation ($\lambda = 0.15406$ nm), in the 2θ range 10-40°, with a step size of 0.02° and a time per step of 1.5 s. The XRD pattern of the aluminium foil was also recorded.

2.2.12. Biological tests

2.2.12.1. Irritability. The HET-CAM test was performed according to the protocol described in (Garcia et al., 2023) and was used to infer about the nanofibers' ability to induce tissue's irritation in the bed wound. Briefly, fertilized hen's eggs were incubated for 8 days at 37 °C and with a relative humidity of 60 % in an incubator YZ-56S. On the 9th day, the eggs were removed from the incubator, the eggshell was cut with a rotary saw (Dremel 3000 from Breda), the inner membrane was hydrated with 0.9 % NaCl solution and then the eggs were returned to the incubator for 30 min for hydration. To assess the choriallantoic membrane (CAM), the inner membrane was carefully removed. Discs with 6 mm of diameter of the supported nanofibers were placed face down over the CAM and observed for 5 min to verify if and when any of the following processes occurred: haemorrhaging (bleeding for the vessels), lysis (blood vessel disintegration), and coagulation (intra and extra-vascular protein denaturation) (ICCVAM, 2010). NaCl (0.9 %) and NaOH (1 M) solutions (300 μL) were used as negative and positive controls, respectively.

2.2.12.2. Cytotoxicity. Cytotoxicity assay was performed to assess the nanofibers biocompatibility. The assay was conducted by indirect contact using porous cell culture inserts (Transwell®), according to ISO standard 10993–5:2009 (International Organization for Standardization. ISO, 2009). NIH/3T3 fibroblasts were cultured in DMEM, supplemented with 10 % (v/v) bovine calf serum and 1 % (v/v) penicillin–streptomycin solution, at 37 °C in a humidified 5 % CO_2 atmosphere. When a confluent monolayer was achieved, cells were subcultured enabling the maintenance of the culture. Pre-warmed 0.25 % (w/v) trypsin – 0.53 mM EDTA was used to promote the detachment of the cells, which were recovered by centrifugation for 5 min at 125*g* and resuspended in a fresh pre-warmed DMEM supplemented medium. Cells from passage 4 to 6 were harvested, diluted with DMEM to 1 x 10^4 cells per well and seeded in 24-well plates (four replicates). After 24 h incubation at 37 °C under humidified 5 % CO_2, the cell medium was replaced by fresh supplemented DMEM, and the inserts were placed above. Samples (5 mm diameter) were carefully positioned into the inserts and an extra 100 μL of DMEM were poured into each well to cover the sample. A negative control (only DMEM) corresponding to 100 % viability and a positive control (DMEM with 10 % of DMSO) corresponding to a cytotoxic condition were also made. After 24 h incubation under the same conditions, both the inserts and the medium were carefully removed and a MTT solution (0.5 mg/mL prepared in serum-free medium) was added to each well followed by additional 3 h incubation. To dissolve the formazan crystal, a solution containing 0.1 % IGEPAL, 4 mM HCl in isopropanol was used. The absorbance was measured using a microplate reader (Platos R 496) at a wavelength of 595 nm. The percentage of cell viability was determined according to equation (3) (International Organization for Standardization. ISO, 2009):

$$Cellviability(\%) = \frac{100 - Abs_t}{Abs_{nc}} \times 100 \quad (3)$$

where (Abs_t) is the mean value of the absorbance of the test samples subtracted by the mean value of the absorbance of the blanks (controls without cells) and (Abs_{nc}) is the mean value of the absorbance of the negative control.

2.2.12.3. Hemocompatibility. The hemocompatibility assay was performed according to the procedure described in (Meng et al., 2021). Blood was collected from healthy individuals at Serviços de Saúde of Instituto Superior Técnico, Lisboa with informed consent (approved by the Ethical Committee of Egas Moniz, Ref. n◦1047/2022), being stabilized in sodium citrate anti-coagulant vacutainer tubes (Vacustest Kima). Nanofibers supported samples (8 mm diameter discs) were individually placed in falcons containing 5 mL of PBS. A volume of 200 μL of blood was added to each one. Negative and positive controls were prepared by adding the blood only to PBS and to DD water, respectively. After 1 h incubation at 37 °C, the samples were gently removed from the falcons, and the solutions were centrifuged at 3000 rpm for 10 min at room temperature. The supernatants were transferred to a 96-well plate and analysed spectrophotometrically at 540 nm. The percentage of haemolysis was calculated through equation (4) (Mahamuni-Badiger et al., 2020):

$$\text{Hemolysis}\,(\%) = \frac{D_t - D_{nc}}{D_{pc} - D_{nc}} \times 100 \quad (4)$$

where D_t is the absorbance of the test samples and D_{pc} and D_{nc} are the absorbances of the positive and negative control, respectively. The assay was performed in quadruplicate.

2.2.12.4. Antimicrobial activity. The antimicrobial activity of the nanofibers was tested by turbidimetry following the procedure described in (Garcia et al., 2023), against *Staphylococcus aureus* ATCC 6538, *Pseudomonas aeruginosa* ATCC 15442, *Escherichia coli* ATCC

25922, *Streptococcus pyogenes* ATCC 12344, Methicillin Resistant *Staphylococcus aureus* (MRSA), and *Candida albicans* ATCC 10231. Mueller-Hinton Broth (MHB) medium was sterilized in an autoclave at 121 °C and 1 bar for 20 min. The microorganisms were incubated overnight at 37 °C and thereafter the density of inoculum was adjusted to a turbidity of 0.5—1 McFarland (10^8 ufc/mL) in bacteria and 3 McFarland to yeast, by suspending the grown colonies in 0.9 % NaCl sterile solution. Samples (6 mm diameter discs) were placed in individual wells of a 48 well plate, filled with 25 μL of each microorganism suspension diluted in 500 μL of MHB. MHB inoculated with the tested microorganisms was used as positive control and MHB only as negative control. The plates were incubated at 37 °C during 24 h. After that, the nanofibers were removed from the wells and the optical density (OD) of the solutions was measured at a wavelength of 600 nm using a Tecan Microplate Reader (Infinite 200 Pro). All the procedures were carried out under aseptic conditions. The assays were performed in triplicate for all formulations.

2.2.13. Statistical analysis

To conduct statistical analysis, GraphPad Prism software was used. Quantitative data are presented as mean ± standard deviation. Shapiro–Wilk test was used to verify the normality of the results. When normality was verified, one-way ANOVA was applied for multiple comparisons, while *t*-test was used to compare means between two independent groups. When normality failed, Kruskal-Wallis test was applied for multiple comparisons and Mann-Whitney to compare two independent groups. The chosen significance level was 0.05. Statistical disparities between datasets are denoted by asterisks (* $p < 0.05$, ** $p < 0.005$, *** $p < 0.0005$).

3. Results and discussion

Casein presents a globular structure with strong inter- and intramolecular forces, such as hydrogen bonds and hydrophobic interactions, that are responsible for its high elasticity and structural stability (Rehan et al., 2019). It presents excellent film-forming abilities, good barrier properties, and the ability to encapsulate and release bioactive compounds, which turns it quite attractive to produce wound dressings. However, electrospinning it by itself to produce nanofibrous structures that can simulate the ECM is challenging, since beads and droplets are formed instead of continuous fibres (Xie and Hsieh, 2003). The mixture with other polymer, like PVA, which has the capacity to form secondary bonds with proteins, reduces these forces and provides the necessary mechanical properties and viscosity to produce stable, continuous electrospun fibres (Xie and Hsieh, 2003). The incorporation of antimicrobial agents that allow to effectively tackle infections at the wound site, is a significant added value for the treatment of diabetic wounds. In this work, a comprehensive assessment was conducted to analyse the physical–chemical and biological attributes of the CAS/PVA nanofiber based systems loaded with different antimicrobial compounds.

3.1. Viscosity

The results of the viscosity measurements of the polymeric solutions used to produce the nanofibers are shown in shown in Fig. 4. The CAS/PVA showed a viscosity of 26.67 ± 0.56 mPa.s. The addition of Octiset®, Polyhexanide and Zinc oxide increased the average viscosity to 35.70 ± 3.45 mPa.s, 27.93 ± 4.12 mPa.s and 30.70 ± 0.53 mPa.s, respectively. However, only in the case of the formulation containing Octiset® the value could be considered statically different from CAS/PVA ($p = 0.011$). The obtained values are compatible with those required for electrospinnable solutions and are of the same order of magnitude as those reported for casein-PEO and casein-PVA solutions used for similar purposes (Selvaraj et al., 2018; Xie and Hsieh, 2003).

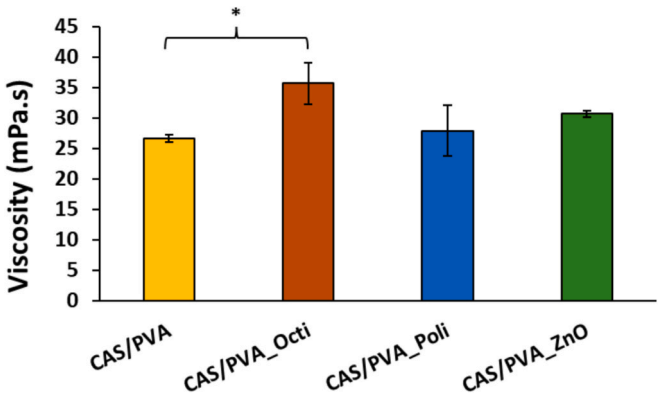

Fig. 4. Viscosity of the polymeric solutions used to produce the nanofibers (n = 3).

3.2. Morphology

The morphological characteristics of the produced electrospun nanofibers, before and after the crosslinking with glutaraldehyde (GA), are depicted in Fig. 5, and the histograms of the nanofibers diameter distribution in Fig. S1, in Supplementary Information. Although various chemical agents are viable options for crosslinking, GA is one of the preferred choices due to its efficacy, ready availability, straightforward processing, and cost-effectiveness (Teixeira et al., 2021). Furthermore, when utilized as vapor, GA has exhibited diminished or negligible cytotoxic effects (Teixeira et al., 2021). The results of the cytotoxicity tests performed with the different samples are presented and discussed in section 3.7.

CAS/PVA samples present randomly oriented nanofibers with diameter 116 ± 43 nm. The exposure to the crosslinker GA resulted in a broadening of the nanofibers giving rise to a denser structure, in alignment with findings of other published studies (Teixeira et al., 2021).

CAS/PVA_Octi nanofibers show a completely different morphology, with a high number of connected spherical structures attached to thinner fibres. Following crosslinking (CAS/PVA_Octi_GA), the material's coalescence increased, being visible larger agglomerates (Teixeira et al., 2021).

CAS/PVA_Poli exhibited a nanofibrous structure punctuated by the occurrence of fusiform-shaped beads. The average fibre diameter measured was 80 ± 25 nm, which is lower than that observed for CAS/PVA. GA led to a denser structure, although its effect was not so pronounced as in the previous cases.

CAS/PVA_ZnO displayed slender fibres with a morphology similar to CAS/PVA_Poli and an average diameter of 79 ± 18 nm. Larger beads, exhibiting a fusiform shape, are visible in this case. The thickening of the beads was even more evident after GA crosslinking than in the previous cases.

Overall, the incorporation of drugs or nanoparticles led to a reduction in fibre diameter, except for CAS/PVA_Octi, whereas crosslinking gave rise to a widening of the structures. Similar trends were reported in the literature for analogous compositions and processing techniques (Xie and Hsieh, 2003; Teixeira et al., 2021; Fong et al., 1999).

It is worth noting that porosity and permeability are key parameters for wound dressing performance, as they influence exudate management, oxygen transport, and drug release. Quantitative porosity and permeability measurements were not feasible due to the thin, adherent nature of the mats. However, SEM observations show that the nanofiber mats, despite their specific characteristics, possess the interconnected and porous structure necessary to maintain a moist and breathable microenvironment, favourable to wound healing, while also supporting adequate diffusion of the released drugs. Future studies shall consider the production of thicker mats that can be detached from the collector material and submitted to oxygen and fluid permeability assays.

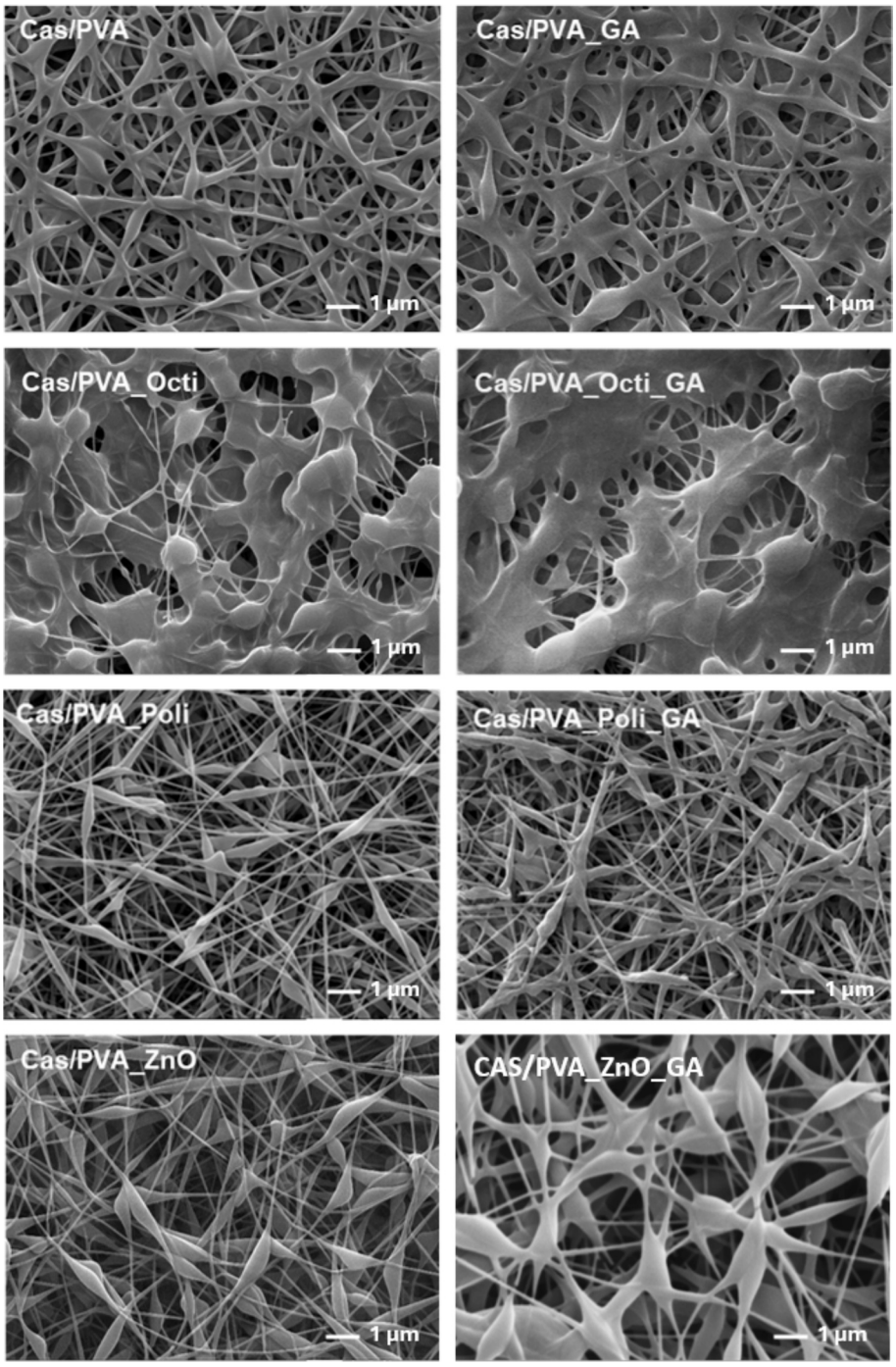

Fig. 5. SEM images of the nanofibers.

3.3. Swelling behavior

Fig. 6 presents the swelling kinetics for the produced nanofibers. In all formulations, the equilibrium state was reached in less than 1 min, indicating that the water absorption into the nanofibers' films was quite fast.

CAS/PVA exhibited an average swelling ratio of 188 %, while CAS/PVA_GA displayed a swelling ratio of 303 %, showing that the swelling capacity notably increased after crosslinking ($p \leq 0.0001$). This unexpected result can be explained by the fact that GA introduces hydrophilic functional groups into the polymer network. The aldehyde groups of GA can react with the amino groups of casein (Głąb and Boratyński, 2017) and hydroxyl groups of PVA (Zhong et al., 2024), forming Schiff bases and acetals/hemiacetals, respectively. These new bonds can increase the hydrophilicity of the polymer network, which leads to higher water absorption and swelling.

The loading of drugs/nanoparticles enhanced the swelling of the samples in comparison to the bare nanofibers. In fact, CAS/PVA_Octi, CAS/PVA_Poli and CAS/PVA_ZnO, absorbed 364 %, 250 %, and 272 % of their dry weight, respectively. This trend might be attributed to the additional water affinity induced by the presence of the drugs/nanoparticles (for example, polyhexanide may form core/shell type micelles, where the hydrophobic segments are oriented towards the centre of the sphere (core), while the hydrophilic groups extend outwards (shell) (de Paula et al., 2011), and/or to the morphological differences relatively to CAS/PVA, which were more evident in the case of CAS/PVA_Octi.

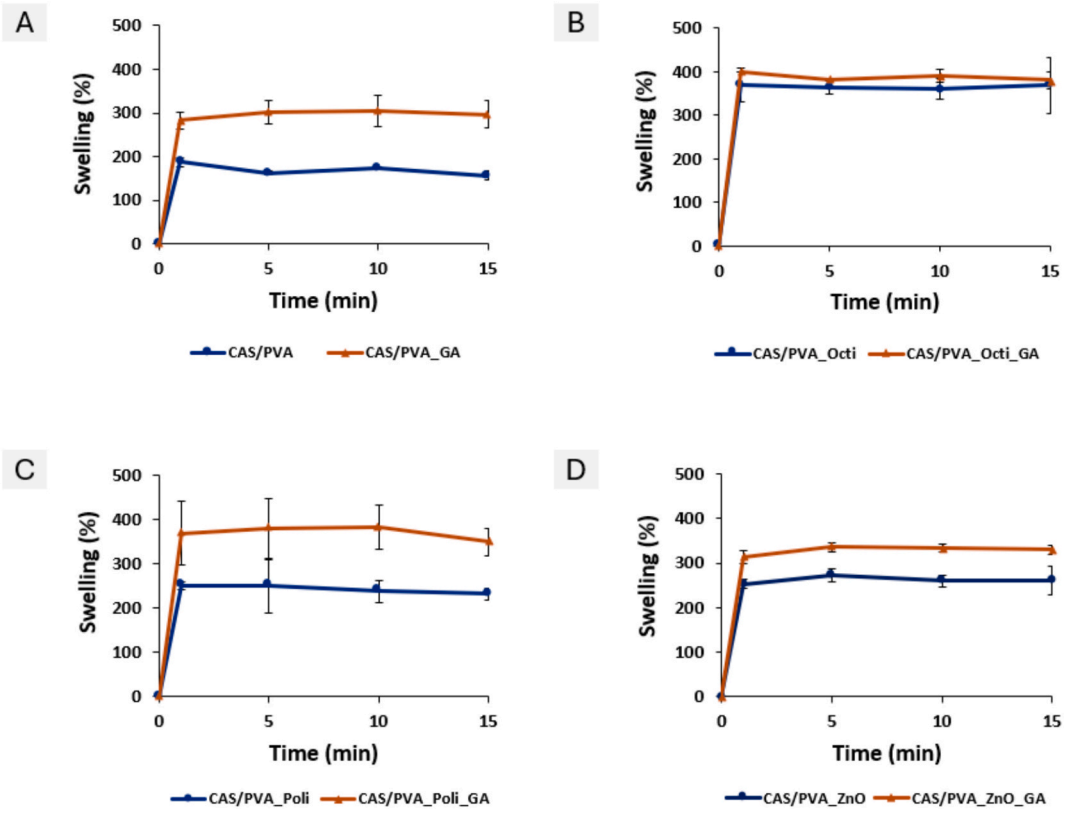

Fig. 6. Swelling ratio of the (A) bare nanofibers and of those containing (B) Octiset®, (C) polyhexanide and (D) ZnO, before and after crosslinking with GA (n = 3).

In agreement with what was observed for CAS/PVA, the crosslinking of the loaded fibres with GA resulted in an increase of the swelling ratio relative to the correspondent non-crosslinked samples. CAS/PVA_Octi_GA, CAS/PVA_Poli_GA and CAS/PVA_ZnO presented swelling ratios of 401 % ($p = 0.0061$), 381 % ($p \leq 0.0001$), and 336 % ($p \leq 0.0001$), respectively.

An ideal wound dressing should provide a moist environment to the wound, to prevent dehydration, being simultaneously able of ensuring the exudate absorption. Therefore, it shall have a high swelling ratio (Li et al., 2013). The swelling ratio of commercial wound dressings significantly varies, depending on the material and type of dressing. The values obtained for the studied materials are of the same order of magnitude of those found for several commercial wound dressings (e.g. Hydrosorb®, a polyurethane-polyurea hydrogel dressing, DuoDERM® Extra Thin, a hydrocolloid polyurethane-based dressing or Acticoat*, a rayon/polyester absorbent dressing (Minsart et al., 2022).

3.4. Drug release

The drug release profiles obtained both for non-crosslinked and crosslinked nanofibers loaded with Octiset® and polyhexanide are illustrated in Fig. 7.

The non-crosslinked samples demonstrated a controlled drug release characterized by two different stages: an initial burst with a higher release rate within the first 4–8 h, followed by a slower release till the 24th hour. The initial burst effectively addresses the presence of bacteria within the wound, while the subsequent sustained release helps preventing wound infection, ensuring a proper environment for the wound healing (Amiri et al., 2020). The crosslinked samples exhibited a much lower burst and a significant reduction in the total amount of drug released, which only reached ≈50 % of the amount released by the non-crosslinked samples. This shall be due to the denser structure of the nanofibers matrix after the crosslinking and lower degradation rate (see below) and/or to the eventual reaction of GA with the amine and hydroxyl groups of the drugs that impair the drug release.

Comparing the two active agents of Octiset®, octenidine exhibited a much lower release than phenoxyethanol (Figs. 7 A1 and A2, respectively). This observation is consistent with the proportions of both drugs in Octiset®, which contains 1 mg/mL of octenidine dihydrochloride and 20 mg/mL of phenoxyethanol to increase the solubility of the former drug (which is much less soluble (PubChem Octenidine dihydrochloride; PubChem Phenoxyethanol), and consequently the efficacy of the antiseptic solution, since octenidine presents a much superior antimicrobial activity (Grecka and Szweda, 2021).

As for polyhexanide (Fig. 7 B), the amounts released are of the same order of magnitude of phenoxyethanol. It shall be stressed that the concentration of polyhexanide used in the preparation of the nanofibers is the same of octenidine (1 mg/mL). The higher amount of polyhexanide released can be related with its higher solubility (PubChem Octenidine dihydrochloride; Summary, 2024) and/or lower affinity to the polymeric matrix. Besides, the fact that the CAS/PVA_Octi and CAS/PVA_Octi_GA present a denser matrix than CAS/PVA_Poli and CAS/PVA_Poli_GA, with coalescing agglomerates, may have impaired the liquid access and the consequent drug release.

3.5. Degradation behavior

Fig. 8 shows the weight loss (%) of the produced nanofibers after being in contact with a saline solution containing an enzyme. The proteases existent in exudate varies, depending on the wound type and stage. The most common ones are matrix metalloproteinases and serine proteases. In the present work, it was used a serine protease (protease XIV) which can cleave peptide bonds (Brown et al., 2015), as those find in casein.

CAS/PVA nanofibers showed a weight loss of 54 %, while the crosslinked system, as expected, presented a lower value (38 %). The incorporation of Octiset® almost did not change the degradation rate of the material, both before and after exposure to GA. The materials

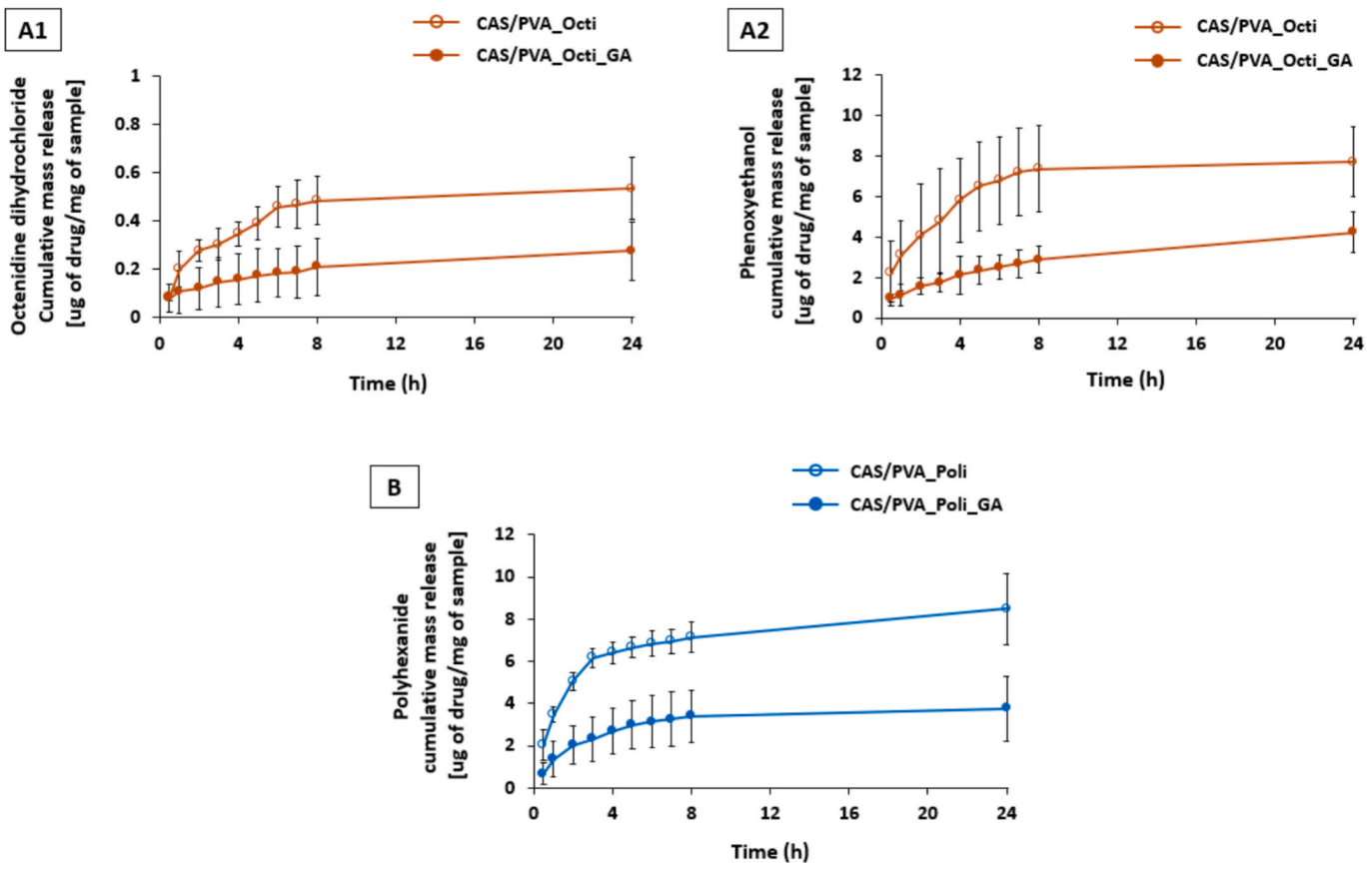

Fig. 7. Cumulative mass released of (A1) octenidine dihydrochloride and (A2) 2-phenoxyethanol from CAS/PVA_Octi and CAS/PVA_Octi_GA, and of (B) polyhexanide from CAS/PVA_Poli and CAS/PVA_Poli_GA ($n \geq 3$).

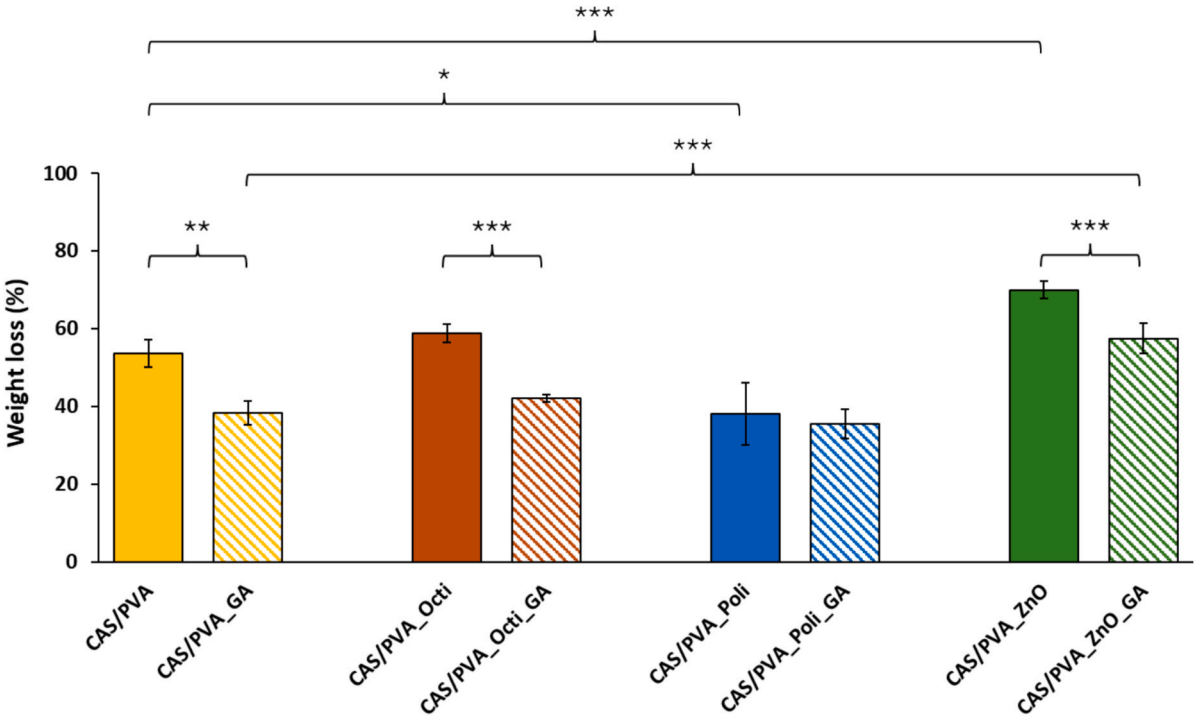

Fig. 8. Degradation of the nanofibers in PBS containing 0.2 mg/mL of protease enzyme XIV solution, in 24 h ($n \geq 3$).

containing polyhexanide suffered the lowest degradation: 38 % in the case of Cas/PVA_Poli and 35 % for CAS/PVA_Poli_GA. CAS/PVA_ZnO and CAS/PVA_ZnO_GA showed a weight loss of 70 % and 56 %, respectively. The lowest degradation of electrospun PVA nanofibers crosslinked with GA vapor was also observed by other authors (Çay et al., 2014; Li et al., 2013), being attributed to the establishment of intermolecular bonds between GA and the constituents of the nanofibers that increases the chemical resistance of the materials. As for the effect of the different drugs/nanoparticles, it is not possible to establish a direct relation between the degradation extent and the morphology of the samples. In fact, the samples containing Octiset® present large agglomerates, which lead to a lower effective contact area of the material with the solution than the remaining samples with a more fiberform structure. However, CAS/PVA_Octi and CAS/PVA_Octi_GA did not present the lowest degradation, as expected. This suggests that the degradation shall be determined by the nature of the added bioactive compound and by the interaction that these can establish with the polymeric matrix. It is interesting to note that the samples containing ZnO particles exhibit the highest degradation values. ZnO particles, being insoluble at neutral pH, might disrupt the polymer matrix, while polyhexanide and the components of Octiset® (octenidine dihydrochloride and 2-phenoxyethanol) might integrate more uniformly within the polymeric matrix, resulting in a structure more resistant to degradation.

Overall, the obtained results indicate that the nanofibers shall undergo partial degradation within 24 h when in contact with exudate enzymes, which is consistent with their intended use as removable wound dressings for chronic wounds requiring frequent replacement. The observed degradation is advantageous, as it promotes the release of bioactive compounds and casein-derived peptides, which may exert antimicrobial, antioxidant, and anti-inflammatory activities. At the same time, the nanofiber's mats shall retain sufficient short-term stability for clinical handling when supported on a backing material, thus ensuring both functional performance and therapeutic benefit. It is worth nothing that although degradation behaviour may affect significantly the performance of the materials, several other factors (e.g., the nature of the incorporated bioactive agents, their concentration, the presence of other compounds) shall also play a key role.

3.6. Irritability

HET-CAM tests are an unexpensive and simple alternative to pre-evaluate biomaterials irritability potential before animal experimentation that, although are mainly used for materials intended for ocular applications, can be extended to materials in contact with other vascularized tissues (Garcia et al., 2023; Oliveira et al., 2020).

Fig. 9 presents the outcomes of the tests. The nanofiber samples were positioned on the chorioallantoic membrane (CAM) surface of fertilized chicken eggs and observed for a 5 min regarding the appearance of signs of hemorrhage (manifested as vessel bleeding), lysis (dissolution of blood vessels), and coagulation (denaturation of intra and extra-vascular proteins). None of the formulations induced changes in the membrane, mirroring the response observed in the negative control. In contrast, the positive control, performed with a solution of NaOH, exhibited extensive hemorrhaging and irritation.

The obtained results point out to a non-irritant behavior of the materials when placed over the wounds, underscoring their potential utility for applications in dressings.

3.7. Cytotoxicity and hemocompatibility

The percentage of cellular viability for the different nanofibers is depicted in Fig. 10 A. As per existing literature, a viability reduction to below 70 % indicates cytotoxic potential (International Organization for Standardization. ISO, 2009). Based on the findings, only the CAS/PVA_Octi_GA formulation demonstrated potential cytotoxicity, as its cell

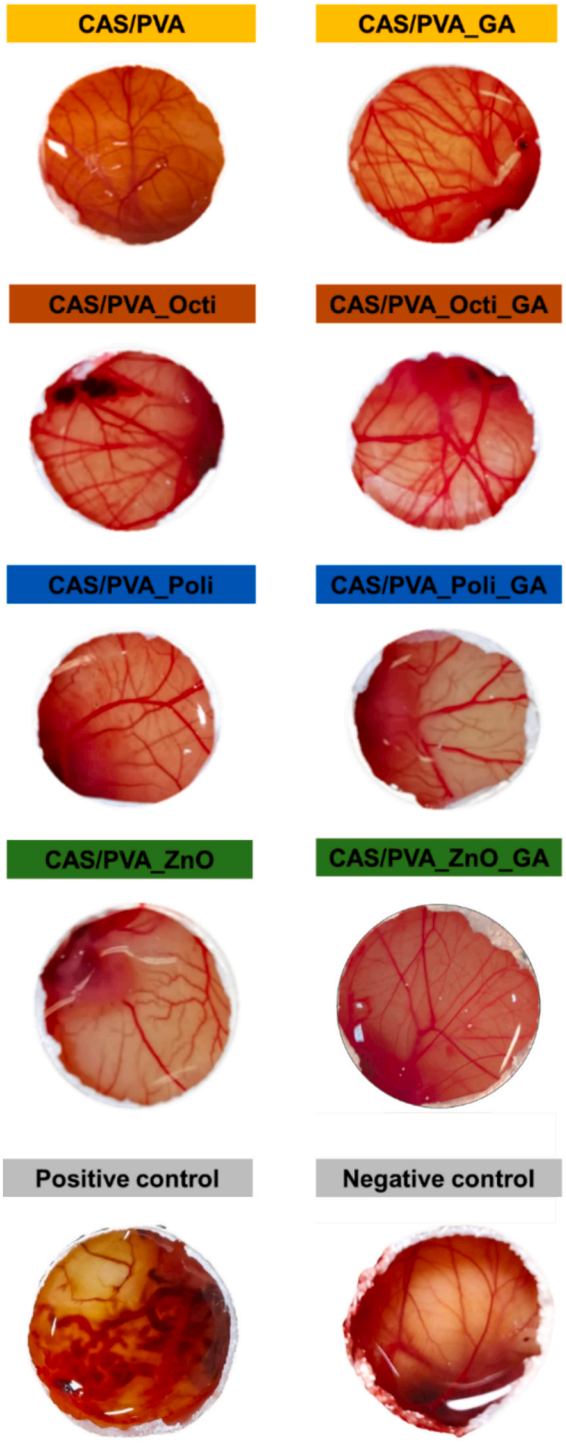

Fig. 9. Chorioallantoic membrane images after 5 min contact with the different samples.

viability dropped below 70 %. This observation could be attributed to a synergistic effect of the presence of glutaraldehyde and of the constituent drugs of Octiset®. In fact, GA is widely used as crosslinker agent for bioartificial devices. Although it has been shown to enhance stability and reduce immunogenicity, it may induce some local cytotoxicity if not neutralized properly (Pal et al., 2009). Also, octenidine hydrochloride and 2-phenoxyethanol, as any other drugs, have toxicity limits that depend on the type of cells with which interact. Kramer *et al.* state that octenidine leads to higher cytotoxicity and retards wound contraction without histological alterations when compared to polyhexanide

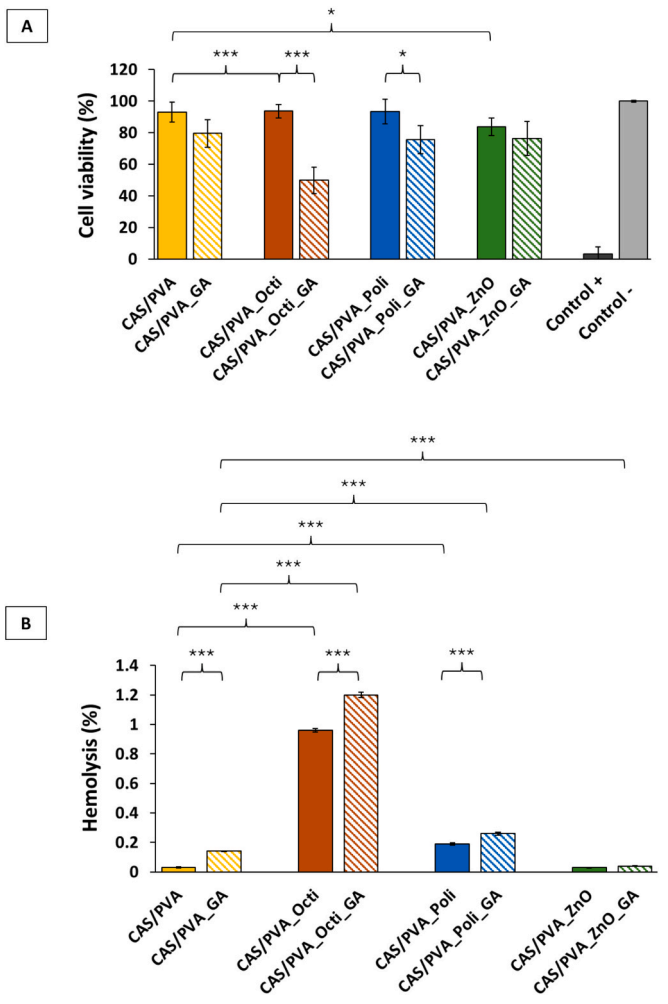

Fig. 10. (A) Cytotoxicity and (B) hemocompatibility of the nanofibers against different microorganisms (n = 4).

(Kramer et al., 2004), but in a posterior study where a significant number of antiseptic agents were tested, including polyhexanide, povidone-iodine and chlorhexidine digluconate, concluded that octenidine presents the highest biocompatibility index (Müller and Kramer, 2008). Sthal *et al.* (Stahl et al., 2010) evaluated the effect of the combination of 0.1 % octenidine and 2 % phenoxyethanol (as in Octiset®) in a porcine wound model and verified that neither retardation of reepithelization nor increased duration of inflammation parameters occurred, highlighting the high *in vivo* biocompatibility of the formulation. Although in the present study the fibres CAS/PVA_Octi_GA may be considered cytotoxic, it shall be stressed that the separate formulations CAS/PVA_GA and CAS/PVA_Octi exhibited no cytotoxic effects, substantiated by their respective cell viability readings. The remaining formulations registered cell viability values above 70 %, indicating their non-cytotoxic nature and thus suggesting their potential safety for employment in wound dressing applications due to their commendable biocompatibility.

It is worth noting that, while the MTT assay provided a reliable measure of acute cytotoxicity and metabolic activity, it does not assess long-term proliferative capacity. Future studies incorporating a colony-formation assay could help distinguish between transient (static) and irreversible (cidal) effects of the nanomaterials on fibroblast viability.

The results of the hemocompatibility assay are also presented in Fig. 10 B. An haemolysis percentage lower than 2 % allows to classify the materials as non-haemolytic, whereas for a range of 2–5 % they are designated as slightly haemolytic, and for values surpassing 5 % are considered haemolytic (Mahamuni-Badiger et al., 2020). The hemolysis percentages for the studied materials are all $\leq$ 1.20 %. An increase in hemolysis percentage was noted following the crosslinking of the nanofibers. However, all formulations remained confined within the spectrum of haemolysis values that align with biomaterials exhibiting hemocompatibility, holding substantial potential for application in wound dressing applications.

3.8. Antimicrobial activity

The antimicrobial efficacy of electrospun nanofibers was assessed against different microorganisms and the results are resumed in Fig. 11.

The non-crosslinked samples prepared with polyhexanide and Octiset® present in general a higher antimicrobial activity than those prepared with ZnO. CAS/PVA_Poli shows a superior performance against *C. albicans, S. pyogenes* and *MRSA,* while CAS/PVA_Octi are better against *E.coli, S.aureus* and *P. aeruginosa.* However, the antimicrobial activity against the last is quite reduced, which may be due to the known resistance of this microorganism to many antimicrobials, namely antiseptics, resultant from the lower permeability of its external membrane and from the presence of over expressed active efflux pumps (Pachori et al., 2019). The observed differences can be attributed to distinct mechanisms of action of the loaded agents which determine its antimicrobial spectrum and efficacy and also to the used concentrations. In any case, it should be noted that *MRSA* is quite dangerous in diabetic wounds due to its resistance to treatment and ability to cause severe infections. Also, *Streptococcus pyogenes* is very dangerous, especially because it can cause necrotizing fasciitis. ZnO nanoparticles are known to possess antimicrobial properties, but their activity may be less broad-spectrum than those of polyhexanide and octenidine (the main active agent in Octiset®) (Babalska et al., 2021). Both polyhexanide and octenidine can disrupt the cell membranes increasing its permeability (Guiomar and Urbano, 2022). However, polyhexanide induces chromosome condensation in bacteria, leading to cell death (Chindera et al., 2016), while octenidine interferes with microbial metabolism by affecting enzymes responsible for critical metabolic pathways (Malanovic et al., 2022). In contrast, ZnO nanoparticles primarily exert their antimicrobial effect through the generation of reactive oxygen species (ROS) and the release of Zn^{2+} ions, which can damage bacterial cell membranes and DNA (Yin et al., 2010). The effectiveness of ZnO nanoparticles can be influenced by factors such as particle size, concentration, and the presence of other substances. Concerning the samples crosslinked with GA, a lower antimicrobial efficacy was generally found. This can be attributed to the lower degradation of these samples (Fig. 8) and to the lower amounts of released drugs (Fig. 7). These effects must overlap to any eventual toxicity of GA.

It shall be stressed that, although the performed tests have provided information about fungistatic and bacteriostatic activity, to address the microbicidal activity, future studies involving the evaluation of CFU counts could be performed.

3.9. Complementary characterization of the best performing systems

The samples with the best antimicrobial behaviour (CAS/PVA_Octi and CAS/PVA_Poli) were further characterized by FTIR spectroscopy and XRD, to try to get more insight into the chemical interactions between the polymeric matrix and the drugs and the crystalline/amorphous nature of the nanofibers. For comparison purposes, CAS/PVA was also analysed. Besides, the mechanisms associated to the release of the drugs from the nanofibers mats were also analysed using different kinetic models.

3.9.1. Chemical structure

The FTIR spectra of CAS/PVA_Octi and CAS/PVA_Poli samples are compared with the one of CAS/PVA in Fig. 12A and 12B, respectively. Fig. S2, in Supplementary Information contains the spectra of the raw

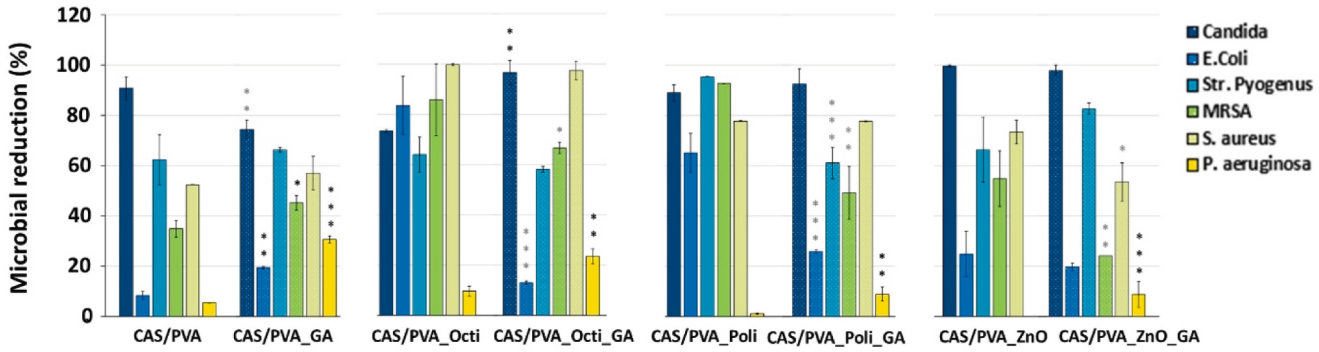

Fig. 11. Antimicrobial activity of the nanofibers non-crosslinked and crosslinked with GA, against different microorganisms. Asterisks indicate statistical differences between the non-crosslinked and the crosslinking sample: black refer to an increase in the antimicrobial effect, while grey indicate a decrease (n = 4).

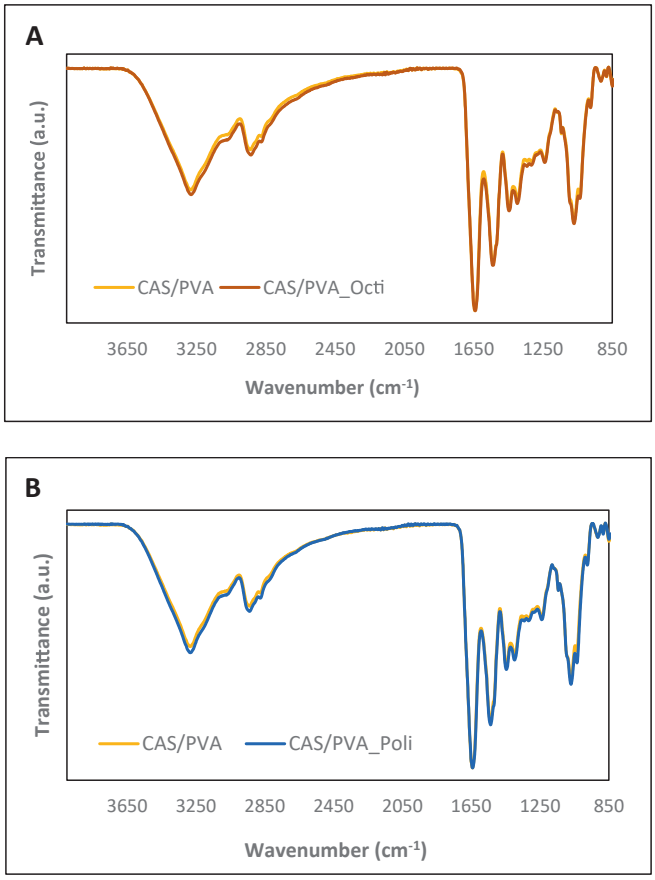

Fig. 12. FTIR-ATR spectra of (A) CAS/PVA_Octi vs CAS/PVA and (B) CAS/PVA_Poli vs CAS/PVA and, in the region of 4000–850 cm^{-1}.

materials used in the production of the nanofibers, namely triethanolamine, PVA, casein, the commercial solution Octiset® and polyhexanide. Spectral data below 850 cm^{-1} were excluded due to a high signal-to-noise ratio which hindered meaningful analysis.

The spectrum of the CAS/PVA fibres displays a broad band between 3550 and 3200 cm^{-1}, attributed to O–H stretching from intra- and intermolecular bonds, overlapping with N–H stretching vibrations from casein. The absorption peak at 2943 cm^{-1} corresponds to C–H stretching of aliphatic groups (–CH_2 or –CH) from the backbone of both polymers, while the peaks at 1635 cm^{-1} and 1538 cm^{-1} are characteristic of the amide I and amide II bands of casein, associated with C=O stretching and N–H bending/C–N stretching vibrations, respectively. The existence of several shifts and the appearance of new bands between 1400 and 1000 cm^{-1} indicate possible interactions and complex formation between PVA and casein through hydrogen bonding involving hydroxyl and amide groups. Indeed, in this region, FTIR spectra contains peaks correspondent to C–O, C–N, and C–C stretching vibrations as well as C–H bending, all sensitive to hydrogen bonding or molecular interactions (Rainho et al., 2025; Karydis-Messinis et al., 2024).

Octiset® spectrum (Fig. S2) exhibits a broad N–H and O–H stretching band around 3326 cm^{-1} and another centred at 1647 cm^{-1} most likely due to C=O stretch from amide I functional groups of cocamidopropyl betaine, a excipient present in the formulation. Much smaller peaks are visible at 1541 cm^{-1}, which can be attributed to amide II also present in the surfactant, and 1149 cm^{-1} due to C–H bending. According to Octiset® fabricant, the main bioactive agents present in this antiseptic solution are phenoxyethanol and octenidine dihydrochloride, being their concentration 20 mg/mL and 1 mg/mL, respectively. Since the amount of octenidine is quite small, it shall not be detected in the spectrum of CAS/PVA_Octi. However, phenoxyethanol amount in the nanofibers is the same as PVA, thus, some of its peaks should be visible. In a study of Badawi (Badawi, 2011), the following vibrational bands were identified in the spectrum of phenoxyethanol: O–H stretching vibration around 3340 cm^{-1}, aliphatic C–H stretching at 2930 and 2873 cm^{-1}, aromatic C=C stretching bands near 1597 and 1495 cm^{-1} and C–O stretching vibrations from the ether and alcohol groups at 1241 and 1040 cm^{-1}. These characteristic signals are largely masked by overlapping bands from CAS and PVA, hindering the clear identification of structural modifications related to the drug incorporation.

Similarly, the spectra of CAS/PVA_Poli and CAS/PVA aro also are also practically indistinguishable. Polyhexanide displays characteristic N–H stretching peaks at 3421 cm^{-1}, which are overshadowed by the broad O–H/N–H band of the PVA/CAS matrix between 3550 and 3200 cm^{-1}. Other polihexanide-associated absorptions, such as C=N stretching (1637 cm^{-1}) and the bending vibration of NH_2^+ (1549 cm^{-1}) are likewise obscured, making direct spectral assignment challenging (Ahani et al., 2017).

Overall, the FTIR analysis revealed clear evidence of intermolecular interactions between PVA and CAS in the electrospun fibres. More, the spectra suggest strong non-covalent interactions (mainly hydrogen bonding and possible electrostatic attractions) between the matrix components and the antiseptic agents, supporting their successful incorporation and sustained release.

3.9.2. *Crystallinity*

The XRD patterns of CAS/PVA_Poli and CAS/PVA_Octi samples are presented in Fig. 13. For comparison purposes, CAS/PVA samples were also analysed. Due to the low thickness of the nanofibers mat, it is possible to identify peaks arising from the support material (aluminium foil), e.g., the high intensity peak observed at ≈ 38.7°. A shallow peak is observed close to 20° in CAS/PVA, which can be attributed to the presence of amorphous casein and semi-crystalline PVA (Biranje et al.,

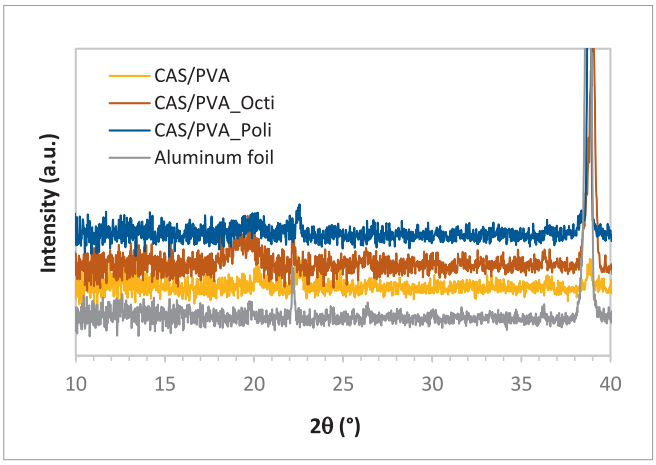

Fig. 13. X-ray diffraction patterns of CAS/PVA, CAS/PVA_Poli and CAS/PVA_Octi samples. Aluminium foil diffractogram is also presented.

2019). The increased intensity and broadening observed for this peak in CAS/PVA_Poli suggests an increase in the fraction of amorphous phases. This is even more significant in CAS/PVA_Octi indicating a decrease in overall crystallinity, which may be attributed to a decrease in the crystallinity of PVA and/or to the presence of other amorphous phases in the composition of the nanofibers.

3.9.3. Drug release mechanisms

The drug release profiles from the nanofibers were fitted to established mathematical models (Higuchi, Korsmeyer-Peppas, Peppas-Sahlin, Kopcha, and Weibull (Corsaro et al., 2021; Kamalpour et al., 2025) to infer about the mechanisms governing the drug release behavior, in particular to determine if it is controlled by diffusion, relaxation/degradation, erosion or occurs due to a combination of these processes. Table 1 presents mathematical expressions correspondent to those models (where M_t/M_∞ is the ratio between the mass of drug released at time t and as the time approaches infinity), and the fitting parameters and correlation coefficient (R^2) for each case.

In Higuchi model, K_H is the Higuchi release constant related to the drug's diffusivity, solubility, and the structural characteristics of the polymeric matrix. In Korsmeyer-Peppas model, K is the kinetic constant incorporating structural and geometric characteristics of the system, and n is the release exponent that characterizes the drug release mechanism ($n < 0.45$: Fickian diffusion; $0.45 < n < 0.89$: non-Fickian (anomalous) transport; $n = 0.89$: relaxation-controlled; $n > 0.89$: erosion/degradation controlled). In Peppas-Sahlin model, K_1 and K_2 are the Fickian diffusion and relaxation/erosion rate constants, respectively, and m is the diffusion exponent. The relative magnitude of K_1 and K_2 indicates the dominant mechanism ($K_1 > K_2$: diffusion-controlled; $K_2 > K_1$: erosion-controlled; $K_1 \approx K_2$: combined diffusion/erosion mechanism). In Kopcha model, A and B are constants representing the diffusion and erosion rate contributions, respectively. The ratio A/B determines the prevailing mechanism: $A/B > 1$: diffusion-controlled; $A/B < 1$: erosion-controlled; $A/B = 1$: equal contribution of both mechanisms. Finally, in Weibull model, τ is the scale constant that represents the time parameter related to the half-release time (t_{50}), and β is the shape parameter that characterizes the release mechanism and curve profile ($\beta < 1$: the release rate decreases with time, typical of diffusion-controlled processes; $\beta = 1$: the release follows an exponential or first-order behaviour; $\beta > 1$: the release presents a sigmoidal profile, suggesting a complex kinetics, often associated with polymer relaxation, degradation, or erosion mechanisms).

The fittings to the Higuchi model led to high R^2 values (≥ 0.93) suggesting a strong diffusional contribution during the initial stages of release. The release constants (k_H) between 0.039 and 0.048 further support a diffusion-controlled mechanism, where drug transport occurs

Table 1
Kinetic parameters obtained by fitting the drug release data to the Higuchi, Korsmeyer-Peppas, Peppas-Sahlin, Kopcha models and Weibull models for (A) CAS/PVA_Poli and (B) CAS/PVA_Octi.

Model	$\frac{Mt}{M\infty}$	Parameter	Polyhexanide (A)	Phenoxyethanol (B)	Octenidine dihydrochloride (B)
Higuchi*	$K_H t^{\frac{1}{2}}$				
		K_H	0.048	0.042	0.039
		R^2	0.958	0.972	0.931
Korsmeyer-Peppas*	Kt^n				
		K	0.029	0.031	0.036
		n	0.620	0.579	0.516
		R^2	0.990	0.828	0.932
Peppas-Sahlin**	$K_1 t^m + K_2 t^{2m}$				
		K_1	0.086	0.068	0.048
		K_2	−0.002	−0.001	−0.0006
		m	0.416	0.451	0.497
		R^2	0.953	0.948	0.950
Kopcha**	$At^{\frac{1}{2}} + Bt$				
		A	0.051	0.051	0.047
		B	−0.0006	−0.0006	−0.0005
		R^2	0.922	0.938	0.949
Weibull**	$1 - e^{\left[-\left(\frac{t}{\tau}\right)^{\beta}\right]}$				
		τ	3.30	5.53	8.34
		β	0.584	0.632	0.748
		t_{50}***	1.76	3.10	5.11
		R^2	0.980	0.982	0.985

*until 60% release.
**complete release profile.
***Determined by $t_{50} = \tau[\ln(2)]^{\frac{1}{\beta}}$.

mainly through the aqueous channels formed within the swollen network. Regarding the Korsmeyer-Peppas model, R^2 values are also superior to 0.93 (except for phenoxyethanol). Since the release exponents assume values between 0.516 and 0.620, the release mechanism can be classified as anomalous (non-Fickian), indicating that both diffusion and polymer chain relaxation contribute to the overall release process. As for the Peppas-Sahlin model, the diffusion and relaxation rate constants (K_1 and K_2, respectively) provide further insights. The reduced negative values of K_2 (from − 0.0006 to − 0.002) indicate that the relaxation/erosion contribution to the release is neglectable, reinforcing that the process was mainly governed by diffusion ($k_1 \gg |k_2|$). The diffusion exponent (m) ranged between 0.416 and 0.497, consistent with the results obtained from the Korsmeyer-Peppas model, and supporting the predominantly diffusion-controlled release behavior. Kopcha model confirms this conclusion, as A values (0.047 to 0.051) are significantly higher than B values (−0.0005 to − 0.0006). The fact that the latter are very small and slightly negative reflects minor statistical deviation rather than a physical erosion effect. Thus, it points to a diffusion-dominated release mechanism for all three drugs, corroborating that erosion or degradation was not the controlling mechanism under the experimental tested conditions. The Weibull model provided a more comprehensive description of the overall release kinetics and presents in general the best fit for all systems. The β values lower than 1 (0.58–0.75) indicate a decelerating diffusion-controlled release kinetics, consistent with the diffusion-relaxation behaviour inferred from the other models. Polyhexanide exhibited the fastest release ($t_{50} = 1.76$ h) which can be attributed largely to its high solubility (National Library of Medicine, 2025), while octenidine release was the slowest ($t_{50} = 5.11$ h) due to partial retention within the hydrophobic domains of the polymeric matrix. It should be stressed that interpretating the differences in the drug release behaviour is a complex task, as it results from the combined influence of multiple physicochemical factors. Molecular charge, size, and solubility govern how easily a compound diffuses through the network, while its specific affinity for the polymer matrix, through electrostatic, hydrophobic, or hydrogen-bonding interactions, further modulates mobility and retention. Therefore, conclusions regarding the main factors that govern the release behaviour should be drawn carefully, considering the multifactorial nature of the process.

4. Conclusions

This study demonstrates the successful fabrication of casein/poly (vinyl alcohol) (CAS/PVA) electrospun nanofibers incorporating Octiset®, polyhexanide, or zinc oxide (ZnO) for use as multifunctional antimicrobial wound dressings. The properties of the nanofiber mats were evaluated before and after crosslinking with glutaraldehyde (GA) vapor. None of the systems exhibited cytotoxicity, except for CAS/PVA_Octi_GA, in which the synergistic effect of the crosslinker and the drug likely accounts for the observed reduction in cell viability. All formulations were non-irritant and hemocompatible. The materials displayed nanofibrous architectures resembling the extracellular matrix, swelling capacities of 188–401 % suitable for exudate absorption and maintenance of a moist wound environment, and degradation rates of 35–70 % (weight loss), sufficient to enable controlled release of the bioactive agents.

Regarding drug-release behavior, the nanofibers containing Octiset® and polyhexanide provided sustained release of the antiseptics over the first 4–8 h, and in some cases up to 24 h at a lower rate. Fitting the release profiles to different kinetic models indicated that the release process is mainly governed by non-Fickian (anomalous) diffusion. As expected, the amount of drug released was significantly lower in the crosslinked samples, which exhibited greater resistance to degradation. Finally, all drug-loaded nanofibers displayed antimicrobial activity against various microorganisms (Gram-negative and Gram-positive bacteria and yeast), with CAS/PVA_Poli and CAS/PVA_Octi emerging as the most promising systems.

Overall, the results showed that:

- CAS/PVA_Poli presented a homogeneous nanofibrous morphology with the most stable structure, the lowest degradation rate, and excellent antimicrobial activity against *S. pyogenes*, MRSA, and *Candida albicans*.
- CAS/PVA_Octi demonstrated strong antibacterial activity against *E. coli* and *S. aureus*, but its morphology displayed large surface agglomerates, which limited mechanical homogeneity and led to faster degradation.
- CAS/PVA_ZnO, despite its high degradation rate, showed the weakest antimicrobial efficacy, likely due to the limited diffusion of Zn^{2+} ions from the insoluble ZnO nanoparticles at neutral pH.

These findings confirm that the composition of the nanofiber matrix directly governs drug-polymer interactions, swelling-degradation balance, and, consequently, the release and biological performance. The synergistic effect of polymer composition, hydration, and matrix stability provides an effective design rationale for wound dressings combining rapid initial disinfection with sustained protection.

CRediT authorship contribution statement

D. Nobre: Visualization, Validation, Investigation, Formal analysis, Data curation. **E. Ekoh:** Data curation, Formal analysis, Investigation, Validation, Visualization. **D.C. Silva:** Validation. **A.C. Branco:** Writing – review & editing, Writing – original draft, Visualization, Validation, Data curation. **V. Pais:** Formal analysis. **A. Almeida:** Data curation, Investigation, Methodology, Resources, Writing – review & editing. **H. Barroso:** Writing – review & editing, Resources, Methodology, Investigation, Data curation. **M. Salema-Oom:** Writing – review & editing, Resources, Methodology, Investigation, Data curation. **R. Fangueiro:** Funding acquisition. **R. Colaço:** Resources, Project administration, Funding acquisition. **R. Galante:** Writing – original draft, Supervision, Project administration, Methodology, Funding acquisition, Conceptualization. **A.P. Serro:** Writing – review & editing, Supervision, Resources, Project administration, Methodology, Funding acquisition, Conceptualization.

Declaration of competing interest

The authors declare that they have no known competing financial interests or personal relationships that could have appeared to influence the work reported in this paper.

Acknowledgements

To Fundação para a Ciência e a Tecnologia (FCT) for funding through the unit projects https://doi.org/10.54499/UIDB/00100/2020 and https://doi.org/10.54499/UIDP/00100/2020 (CQE), https://doi.org/10.54499/UIDB/50022/2020 (IDMEC/LAETA), and https://doi.org/10.54499/UIDB/04585/2020 (CiiEM) and the research project Milk4-WoundCare (https://doi.org/10.54499/2022.03408.PTDC). Diana C. Silva acknowledges FCT for her Junior Research contract https://doi.org/10.54499/2022.08560.CEECIND/CP1713/CT0016. Also to Governo Regional dos Açores for funding through the project MilkFiber - ACORES-01-0247-FEDER-000024. Acknowledgements are also due to Eng. Paula Matos from Laboratório de Radioesterilização (C2TN-IST) for the support with gamma irradiation.

Appendix A. Supplementary data

Supplementary data to this article can be found online at https://doi.org/10.1016/j.ijpharm.2025.126320.

Data availability

Data will be made available on request.

References

Ahani, E., Montazer, M., Toliyat, T., Mahmoudi, R.d.M., 2017. A novel biocompatible antibacterial product: Nanoliposomes loaded with poly(hexamethylene biguanide chloride). J. Bioact. Compat. Polym. 32, 242–262. https://doi.org/10.1177/0883911516675367.

Ahmed, J., Guler, E., Sinemcan Ozcan, G., Emin Cam, M., Homer-Vanniasinkam, S., Edirisinghe, M., 2023. Casein fibres for wound healing. J. R. Soc. Interface 20. https://doi.org/10.1098/rsif.2023.0166.

Akkus, G., Sert, M., 2022. Diabetic foot ulcers: a devastating complication of diabetes mellitus continues non-stop in spite of new medical treatment modalities. World J. Diabetes 13, 1106–1121. https://doi.org/10.4239/wjd.v13.i12.1106.

Aliee, F., Fahimirad, S., Ganji, A., Abtahi, H., 2025. Antimicrobial and Wound Healing Performance of Polycaprolactone Electrospun-based Nanofibers Incorporating Propolis and *Quercus Infectoria* Gall Extracts. Nano 20. https://doi.org/10.1142/S1793292024500747.

Amiri, N., Ajami, S., Shahroodi, A., Jannatabadi, N., Amiri Darban, S., Fazly Bazzaz, B.S., et al., 2020. Teicoplanin-loaded chitosan-PEO nanofibers for local antibiotic delivery and wound healing. Int. J. Biol. Macromol. 162, 645–656. https://doi.org/10.1016/j.ijbiomac.2020.06.195.

Aydın, M.S., Eren, M.A., Uyar, N., Kankılıç, N., Karaaslan, H., Sabuncu, T., et al., 2024. Relationship between systemic immune inflammation index and amputation in patients with diabetic foot ulcer. J. Orthop. Sci. 29, 1060–1063. https://doi.org/10.1016/j.jos.2023.07.015.

Babalska, Z.Ł., Korbecka-Paczkowska, M., Karpiński, T.M., 2021. Wound antiseptics and european guidelines for antiseptic application in wound treatment. Pharmaceuticals 14, 1253. https://doi.org/10.3390/ph14121253.

Badawi, H.M., 2011. Vibrational spectra and assignments of 2-phenylethanol and 2-phenoxyethanol. Spectrochim. Acta A Mol. Biomol. Spectrosc. 82, 63–68. https://doi.org/10.1016/j.saa.2011.06.066.

Biranje, S., Madiwale, P., Adivarekar, R.V., 2019. Porous electrospun Casein/PVA nanofibrous mat for its potential application as wound dressing material. J. Porous Mater. 26, 29–40. https://doi.org/10.1007/s10934-018-0602-7.

Bommer, C., Sagalova, V., Heesemann, E., Manne-Goehler, J., Atun, R., Bärnighausen, T., et al., 2018. Global Economic Burden of Diabetes in adults: Projections from 2015 to 2030. Diabetes Care 41, 963–970. https://doi.org/10.2337/dc17-1962.

Brown, J., Lu, C.L., Coburn, J., Kaplan, D.L., 2015. Impact of silk biomaterial structure on proteolysis. Acta Biomater. 11, 212–221. https://doi.org/10.1016/j.actbio.2014.09.013.

Çay, A., Miraftab, M., Kumbasar, P.A., E., 2014. Characterization and swelling performance of physically stabilized electrospun poly(vinyl alcohol)/chitosan nanofibres. Eur. Polym. J. 61, 253–262. https://doi.org/10.1016/j.eurpolymj.2014.10.017.

Chiaula, V., Jeppe Madsen, J., Madsen, F.B., Mazurek, P., Nielsen, A.C., Skov, A.L., 2023. Antimicrobial silicone skin adhesives facilitated by controlled octenidine release from glycerol compartments. Int J Smart Nano Mater 14, 369–389. https://doi.org/10.1080/19475411.2023.2240743.

Chindera, K., Mahato, M., Kumar Sharma, A., Horsley, H., Kloc-Muniak, K., Kamaruzzaman, N.F., et al., 2016. The antimicrobial polymer PHMB enters cells and selectively condenses bacterial chromosomes. Sci. Rep. 6, 23121. https://doi.org/10.1038/srep23121.

Corsaro, C., Neri, G., Mezzasalma, A.M., Fazio, E., 2021. Weibull Modeling of Controlled Drug Release from Ag-PMA Nanosystems. Polymers (basel) 13, 2897. https://doi.org/10.3390/polym13172897.

Da Silva, J., Leal, E.C., Carvalho, E., Silva, E.A., 2023. Innovative Functional Biomaterials as Therapeutic Wound Dressings for Chronic Diabetic Foot Ulcers. Int. J. Mol. Sci. 24. https://doi.org/10.3390/ijms24129900.

de Paula, G.F., Netto, G.I., Mattoso, L.H.C., 2011. Physical and chemical characterization of poly(hexamethylene biguanide) hydrochloride. Polymers (basel) 3, 928–941. https://doi.org/10.3390/polym3020928.

Diabetes around the world-2024 based on extrapolation from similar countries. https://diabetesatlas.org/media/uploads/sites/3/2025/04/IDF_Atlas_11th_Edition_2025_Global-Factsheet.pdf?utm_source=chatgpt.com (accessed 23/07/2025).

Durmaz, B.U., Aytac, A., 2019. Poly (vinyl alcohol) and casein films: the effects of glycerol amount on the properties of films. Res. Eng. Struct. Mater. 5, 155–165. https://doi.org/10.17515/resm2018.62is0803.

Fahimirad, S., Satei, P., Latifi, A., Changizi-Ashtiyani, S., Bahrami, M., Abtahi, H., 2024. Electrospun PCL/PVA/PHMB nanofibers incorporating Ziziphus jujuba fruit fruit extract as promising wound dressings with potent antibacterial and antidiabetic properties. J. Biomater. Sci. Polym. Ed. 35, 2484–2505. https://doi.org/10.1080/09205063.2024.2384299.

Fitzmaurice, S.D., Sivamani, R.K., Isseroff, R.R., 2011. Antioxidant Therapies for Wound Healing: a Clinical Guide to currently Commercially Available Products. Skin Pharmacol. Physiol. 24, 113–126. https://doi.org/10.1159/000322643.

Fong, H., Chun, I., Reneker, D.H., 1999. Beaded nanofibers formed during electrospinning. Polymer 40, 4585–4592. https://doi.org/10.1016/S0032-3861(99)00068-3.

Garcia, L.V., Silva, D., Costa, M.M., Armés, H., Salema-Oom, M., Saramago, B., et al., 2023. Antiseptic-Loaded Casein Hydrogels for Wound Dressings. Pharmaceutics 15, 334. https://doi.org/10.3390/pharmaceutics15020334.

Grecka, K., Szweda, P., 2021. Synergistic effects of propolis combined with 2-phenoxyethanol and antipyretics on the growth of Staphylococcus Aureus. Pharmaceutics 13, 1–17. https://doi.org/10.3390/pharmaceutics13020215.

Guiomar, A.J., Urbano, A.M., 2022. Polyhexanide-Releasing Membranes for Antimicrobial Wound Dressings: a critical Review. Membranes (basel) 12, 1281. https://doi.org/10.3390/membranes12121281.

Głąb, T.K., Boratyński, J., 2017. Potential of Casein as a Carrier for Biologically active Agents. Top. Curr. Chem. 375. https://doi.org/10.1007/s41061-017-0158-z.

Homaeigohar, S., Boccaccini, A.R., 2020. Antibacterial biohybrid nanofibers for wound dressings. Acta Biomater. 107, 25–49. https://doi.org/10.1016/j.actbio.2020.02.022.

ICCVAM. The Hen's Egg Test –Chorioallantoic Membrane Test Method. ICCVAM Test Method Evaluation Report: Current Validation Status of In Vitro Test Methods Proposed for Identifying Eye Injury Hazard Potential of Chemicals and Products, Research Triangle Park, North Carolina: NIH Publication No. 10-7553. National Institute of Environmental Health Sciences; 2010, p. 19–25.

International Organization for Standardization. ISO 10993-5 Biological evaluation of medical devices - Part 5: Tests for in vitro cytotoxicity 2009.

Kamalpour, R., Koocheki, A., Ghorani, B., 2025. Encapsulation of D-limonene in Lepidium perfoliatum seed gum/PVA electrospun nanofibers: Physicochemical characterization and modeling the kinetics of release. Curr. Res. Food Sci. 10, 100966. https://doi.org/10.1016/j.crfs.2024.100966.

Karydis-Messinis, A., Kyriakaki, C., Triantafyllou, E., Tsirka, K., Gioti, C., Gkikas, D., et al., 2024. Development and Physicochemical Characterization of Edible Chitosan–Casein Hydrogel Membranes for potential use in Food packaging. Gels 10, 254. https://doi.org/10.3390/gels10040254.

Kramer, A., Roth, B., Müller, G., Rudolph, P., Klöcker, N., 2004. Influence of the antiseptic agents polyhexanide and octenidine on FL cells and on healing of experimental superficial aseptic wounds in piglets: a double-blind, randomised, stratified, controlled, parallel-group study. Skin Pharmacol. Physiol. 17, 141–146. https://doi.org/10.1159/000077241.

Kurze, C., Farn, C.J., Siow, J., 2022. The Interdisciplinary Approach: Preventive and Therapeutic strategies for Diabetic Foot Ulcers. Foot Ankle Clin. 27, 529–543. https://doi.org/10.1016/j.fcl.2022.03.001.

Li, C.W., Fu, R.Q., Yu, C.P., Li, Z.H., Guan, H.Y., Hu, D.Q., et al., 2013. Silver nanoparticle/chitosan oligosaccharide/poly(vinyl alcohol) nanofibers as wound dressings: a preclinical study. Int. J. Nanomed. 8, 4131–4145. https://doi.org/10.2147/IJN.S51679.

Liu, S., Qamar, S.A., Qamar, M., Basharat, K., Bilal, M., 2021. Engineered nanocellulose-based hydrogels for smart drug delivery applications. Int. J. Biol. Macromol. 181, 275–290. https://doi.org/10.1016/j.ijbiomac.2021.03.147.

Maaz Arif, M., Khan, S.M., Gull, N., Tabish, T.A., Zia, S., Ullah Khan, R., et al., 2021. Polymer-based biomaterials for chronic wound management: promises and challenges. Int. J. Pharm. 598. https://doi.org/10.1016/j.ijpharm.2021.120270.

Mahamuni-Badiger, P.P., Patil, P.M., Patel, P.R., Dhanavade, M.J., Badiger, M.V., Marathe, Y.N., et al., 2020. Electrospun poly(3-hydroxybutyrate-: Co -3-hydroxyvalerate)/polyethylene oxide (PEO) microfibers reinforced with ZnO nanocrystals for antibacterial and antibiofilm wound dressing applications. New J. Chem. 44, 9754–9766. https://doi.org/10.1039/d0nj01384f.

Mahgoub, U., Magee, M.J., Heydari, M., Choudhary, M., Santamarina, G., Schenker, M., et al., 2022. Outpatient clinic attendance and outcomes among patients hospitalized with diabetic foot ulcers. J. Diabetes Complications 36. https://doi.org/10.1016/j.jdiacomp.2022.108283.

Malanovic, N., Buttress, J.A., Vejzovic, D., Ön, A., Piller, P., Kolb, D., et al., 2022. Disruption of the Cytoplasmic Membrane Structure and Barrier Function Underlies the Potent Antiseptic activity of Octenidine in Gram-positive Bacteria. Appl. Environ. Microbiol. 88. https://doi.org/10.1128/aem.00180-22.

Mariia, K., Arif, M., Shi, J., Song, F., Chi, Z., Liu, C., 2021. Novel chitosan-ulvan hydrogel reinforcement by cellulose nanocrystals with epidermal growth factor for enhanced wound healing: In vitro and in vivo analysis. Int. J. Biol. Macromol. 183, 435–446. https://doi.org/10.1016/j.ijbiomac.2021.04.156.

Meng, X., Lu, Y., Gao, Y., Cheng, S., Tian, F., Xiao, Y., et al., 2021. Chitosan/alginate/hyaluronic acid polyelectrolyte composite sponges crosslinked with genipin for wound dressing application. Int. J. Biol. Macromol. 182, 512–523. https://doi.org/10.1016/j.ijbiomac.2021.04.044.

Miguel, S.P., Sequeira, R.S., Moreira, A.F., Cabral, C.S.D., Mendonça, A.G., Ferreira, P., et al., 2019. An overview of electrospun membranes loaded with bioactive molecules for improving the wound healing process. Eur. J. Pharm. Biopharm. 139, 1–22. https://doi.org/10.1016/j.ejpb.2019.03.010.

Minsart, M., Van Vlierberghe, S., Dubruel, P., Mignon, A., 2022. Commercial wound dressings for the treatment of exuding wounds: an in-depth physico-chemical comparative study. Burns. Trauma 10. https://doi.org/10.1093/burnst/tkac024.

Müller, G., Kramer, A., 2008. Biocompatibility index of antiseptic agents by parallel assessment of antimicrobial activity and cellular cytotoxicity. J. Antimicrob. Chemother. 61, 1281–1287. https://doi.org/10.1093/jac/dkn125.

Musa BH, Hameed NJ, 2021. Effect of crosslinking agent (glutaraldehyde) on the mechanical properties of (PVA/Starch) blend and (PVA/PEG) binary blend films. J Phys Conf Ser, 1795, 012064. https://doi.org/10.1088/1742-6596/1795/1/012064.

National Library of Medicine - National Center of Biotechnology Information. Compound Summary: Polihexanide. Https://PubchemNcbiNlmNihGov/Compound/Polihexanide 2025.

Oliveira, A.S., Schweizer, S., Nolasco, P., Barahona, I., Saraiva, J., Colaço, R., et al., 2020. Tough and low friction polyvinyl alcohol hydrogels loaded with anti-inflammatories for cartilage replacement. Lubricants 8, 1–22. https://doi.org/10.3390/lubricants8030036.

Pachori, P., Gothalwal, R., Gandhi, P., 2019. Emergence of antibiotic resistance Pseudomonas aeruginosa in intensive care unit; a critical review. Genes Dis 6, 109–119. https://doi.org/10.1016/j.gendis.2019.04.001.

Pal, K., Paulson, A.T., Rousseau, D., 2009. Biopolymers in Controlled-Release delivery Systems. Modern Biopolymer Science, Elsevier 519–557. https://doi.org/10.1016/B978-0-12-374195-0.00016-1.

Pouliot, Y., Gauthier, S.F., 2006. Milk growth factors as health products: some technological aspects. Int. Dairy J. 16, 1415–1420. https://doi.org/10.1016/j.idairyj.2006.06.006.

PubChem Compound Summary for Octenidine dihydrochloride 2024.

PubChem Compound Summary for Phenoxyethanol, 2024.

Purup, S., Nielsen, S.D., Le, T.T., Bertelsen, H., Sørensen, J., Larsen, L.B., 2019. Wound Healing Properties of Commercial Milk Hydrolysates in Intestinal Cells. Int. J. Pept. Res. Ther. 25, 483–491. https://doi.org/10.1007/s10989-018-9692-y.

Raha, S., Ahmaruzzaman, M., 2022. ZnO nanostructured materials and their potential applications: progress, challenges and perspectives. Nanoscale Adv. 4, 1868–1925. https://doi.org/10.1039/d1na00880c.

Rainho, P., Salema-Oom, M., Pinto, C.A., Saraiva, J.A., Saramago, B., Silva, D.C., et al., 2025. Polyvinyl alcohol/casein hydrogels with oxymatrine eluting ability for cancer-related wound management. Biomater. Sci. 13, 2755–2766. https://doi.org/10.1039/D5BM00191A.

Rediguieri CF, De Jesus Andreoli Pinto T, Bou-Chacra NA, Galante R, De Araújo GLB, Do Nascimento Pedrosa T, et al. Ozone gas as a benign sterilization treatment for PLGA nanofiber scaffolds. Tissue Eng Part C Methods 2016;22:338–47. https://doi.org/10.1089/ten.tec.2015.0298.

Rehan, F., Ahemad, N., Gupta, M., 2019. Casein nanomicelle as an emerging biomaterial—A comprehensive review. Colloids Surf. B Biointerfaces 179, 280–292. https://doi.org/10.1016/j.colsurfb.2019.03.051.

Sahoo, S., Ang, L.T., Goh, J.C.H., Toh, S.L., 2010. Growth factor delivery through electrospun nanofibers in scaffolds for tissue engineering applications. J. Biomed. Mater. Res. A 93, 1539–1550. https://doi.org/10.1002/jbm.a.32645.

Selvaraj, S., Thangam, R., Fathima, N.N., 2018. Electrospinning of casein nanofibers with silver nanoparticles for potential biomedical applications. Int. J. Biol. Macromol. 120, 1674–1681. https://doi.org/10.1016/j.ijbiomac.2018.09.177.

Shahriar, S.M.S., Mondal, J., Hasan, M.N., Revuri, V., Lee, D.Y., Lee, Y.K., 2019. Electrospinning nanofibers for therapeutics delivery. Nanomaterials 9, 532. https://doi.org/10.3390/nano9040532.

Singer, M.E., Dorrance, K.A., Oxenreiter, M.M., Yan, K.R., Close, K.L., 2022. The type 2 diabetes 'modern preventable pandemic' and replicable lessons from the COVID-19 crisis. Prev. Med. Rep. 25. https://doi.org/10.1016/j.pmedr.2021.101636.

Stahl, J., Braun, M., Siebert, J., Kietzmann, M., 2010. The effect of a combination of 0.1% octenidine dihydrochloride and 2% 2-phenoxyethanol (octenisept®) on wound healing in pigs in vivo and its in vitro percutaneous permeation through intact and barrier disrupted porcine skin. Int. Wound J. 7, 62–69. https://doi.org/10.1111/j.1742-481X.2009.00648.x.

PubChem Compound Summary for Polihexanide 2024.

Szostak, K., Czogalla, A., Przybyło, M., Langner, M., 2018. New lipid formulation of octenidine dihydrochloride. J. Liposome Res. 28, 106–111. https://doi.org/10.1080/08982104.2016.1275678.

Tavakoli, S., Klar, A.S., 2020. Advanced hydrogels as wound dressings. Biomolecules 10, 1–20. https://doi.org/10.3390/biom10081169.

Teixeira, M.A., Antunes, J.C., Amorim, M.T.P., Felgueiras, H.P., 2021. Green Optimization of Glutaraldehyde Vapor-based Crosslinking on Poly(Vinyl Alcohol)/Cellulose Acetate Electrospun Mats for applications as Chronic Wound Dressings. MDPI AG 30. https://doi.org/10.3390/cgpm2020-07193.

Tonda-Turo, C., Ruini, F., Ceresa, C., Gentile, P., Varela, P., Ferreira, A.M., et al., 2018. Nanostructured scaffold with biomimetic and antibacterial properties for wound healing produced by 'green electrospinning. Colloids Surf. B Biointerfaces 172, 233–243. https://doi.org/10.1016/j.colsurfb.2018.08.039.

Xie, J., Hsieh, Y.-L., 2003. Ultra-high surface fibrous membranes from electrospinning of natural proteins: casein and lipase enzyme. J. Mater. Sci. 38, 2125–2133. https://doi.org/10.1023/A:1023763727747.

Yeniay, E., Öcal, L., Altun, E., Giray, B., Nuzhet Oktar, F., Talat Inan, A., et al., 2019. Nanofibrous wound dressing material by electrospinning method. Int. J. Polym. Mater. Polym. Biomater. 68, 11–18. https://doi.org/10.1080/00914037.2018.1525718.

Yin, H., Casey, P.S., McCall, M.J., Fenech, M., 2010. Effects of surface chemistry on cytotoxicity, genotoxicity, and the generation of reactive oxygen species induced by ZnO nanoparticles. Langmuir 26, 15399–15408. https://doi.org/10.1021/la101033n.

Zhang, S., Ge, G., Qin, Y., Li, W., Dong, J., Mei, J., et al., 2023. Recent advances in responsive hydrogels for diabetic wound healing. Mater. Today Bio 18. https://doi.org/10.1016/j.mtbio.2022.100508.

Zhong, Y., Lin, Q., Yu, H., Shao, L., Cui, X., Pang, Q., et al., 2024. Construction methods and biomedical applications of PVA-based hydrogels. Front. Chem. 12. https://doi.org/10.3389/fchem.2024.1376799.